RADC-TR- 64-584
Final Report

INVESTIGATION OF THE STATISTICS OF BREAKDOWN USING NANOSECOND PULSE TECHNIQUES

D. F. McDonald
C. J. Benning
S. J. Brient

TECHNICAL REPORT NO. RADC-TR- 64-584
March 1965

Techniques Branch
Rome Air Development Center
Research and Technology Division
Air Force Systems Command
Griffiss Air Force Base, New York

INVESTIGATION OF THE STATISTICS OF BREAKDOWN USING NANOSECOND PULSE TECHNIQUES

D. F. McDonald
C. J. Benning
S. J. Brient

AIR FORCE, GAFB, N.Y., 21 APR 65-133

FOREWORD

This report was prepared under Contract No. AF30(602)-2781 by Braddock, Dunn and McDonald Inc. of El Paso, Texas.

RADC Project Monitor was Ronald C. Blackall (EMATP); Project Number 4506, Task Number 450603.

This technical report has been reviewed and is approved.

Approved: Ronald C. Blackall
RONALD C. BLACKALL
AlC, USAF
Project Engineer

Approved:
THOMAS S. BOND, JR.
Colonel, USAF
Chief, Surveillance
and Control Division

FOR THE COMMANDER:
IRVING J. GABELMAN
Chief, Advanced Studies Group

ABSTRACT

The experimental equipment, experimental procedures, and test results of a laboratory study of the statistics of discharge initiation in highly over-volted planar spark gaps is presented. The theory of operation of a subnanosecond rise-time multikilovolt pulse generator developed for the study is described. Test data on the electron emission of different electrode materials as a function of gap field strength and electrode conditioning is presented. In addition, a simplified model of the statistics of free-space breakdown in a transmitted microwave beam is developed.

TABLE OF CONTENTS

INTRODUCTION

This report presents results of a 13-month program conducted by Braddock, Dunn and McDonald, Inc. (BDM) to investigate the statistics of gaseous breakdown. The purpose of the program was to achieve a better understanding of gaseous breakdown statistics for use in the development of super-power radar systems.

Previous studies[1,2] have shown that it may be possible to transmit extremely high-power during the total time delay which precedes electrical breakdown. This total time delay is composed of two parts:

a. Statistical time delay

b. Formative time delay

Gould and Roberts[3] have shown theoretically and experimentally the peak power limitations as determined by the formative time for the case of microsecond pulses. Proud and Felsenthal[2] have recently extended this work into the nanosecond region. In previous work conducted by BDM[1] under this program, it was suggested that the average statistical time delay can be made much greater than the formative time delay and permit the design of super-power systems using nanosecond pulse widths. The current program was conducted to investigate the characteristics of statistical time delay in more detail.

In the course of the current investigation, BDM conducted experimental studies of the dependence of statistical time delay on electric

field strength and electrode surface characteristics. To accomplish this, it was necessary to develop a sub-nanosecond rise-time, multikilovolt pulse generator. With this generator it was possible to study breakdown statistics in test gaps in which the voltage applied was as high as 10 times greater than the static breakdown voltage. The studies conducted with this equipment indicate that by electrode "conditioning" the statistical time delay can be increased significantly.

In addition to the studies of the statistics of breakdown in discharge gaps, consideration was also given to breakdown in free space. The results of the preliminary theoretical analysis indicate that breakdown of this type may not be a serious problem in superpower systems.

In the sections which follow, a detailed description of the theory of the experimental apparatus, the experimental procedures, and results of the current program are presented.

SECTION I

THE STATISTICS OF BREAKDOWN

The theory of statistical time lags is based on the fact that two probabilistic events must jointly occur before a breakdown can be initiated. These events are:

a. A free electron must be generated, and

b. The electron must be located in a position which will permit it to initiate an electron avalanche.

In a test gap with planar electrodes every electron generated at the cathode will initiate breakdown when the electric field is at least 25% greater than the static breakdown field, E_s. For the fields considered in this program, the static breakdown field is always exceeded by more than 25%. Therefore, the statistical time lag will depend only on the probability density function which describes the time required for an electron to be emitted from a metal electrode under the influence of a high electric field.

The statistical treatment of the time lag is straightforward. Assume that a large number of trials, n_o, are conducted in which a step function electric field ($>1.25E_s$) is applied to a test gap. If time measurements are begun at the time of the application of the voltage pulses, a number, n, will not have experienced breakdown after an interval of time, t. Then the number, dn, which experiences breakdown in the following small interval of time, dt, is given by,

$$dn = -Indt \tag{1-1}$$

where I is the average number of electrons which appear per second in the gap. The negative sign used in the expression indicates that the number of surviving voltage pulses is reduced by dn during the interval of time, t to t + dt. Integrating equation (1-1) and making use of the fact that at t = 0, n = n_o, one obtains

$$n = n_o e^{-It} \tag{1-2}$$

The number of breakdown events, n_B, which occur in the time interval o to t is found by subtracting equation (1-2) from n_o. This yields

$$n_B = n_o (1 - e^{-It}) \tag{1-3}$$

Rearranging this equation gives

$$\frac{n_B}{n_o} = F(t) = 1 - e^{-It} \tag{1-4}$$

where F(t) is the probability distribution function for the number of breakdowns as a function of the interval 0 to t. The density function is

$$\frac{dF(t)}{dt} = Ie^{-It} = f(t) \tag{1-5}$$

and the expected value of t, which is the statistical time lag, t_s, is

$$t_s = \int_o^\infty t\, f(t)\, dt = \frac{1}{I} \tag{1-6}$$

In the experimental work conducted under this program, a test gap using Rogowski electrodes[4] was used. The gap spacing was small and the

volume between the gaps was small. No artificial radiation was introduced into the gap. Accordingly, for the high electric fields applied it was assumed that all discharge-initiating electrons were emitted from the cathode of the gap. It was also assumed that the theory presented above applied to these conditions.

SECTION II

APPARATUS AND INSTRUMENTATION

A. Apparatus Description and Operation

To investigate the statistical delay for highly over-volted planar gaps it was necessary to design a kilovolt generator with the capability of providing a step-function pulse with a sub-nanosecond rise time. Devices employing commercially available thyratrons or spark gaps fall considerably short of this rise time requirement. Fletcher[5] has developed a sub-nanosecond rise time kilovolt generator using a high-pressure, triggered spark gap and commercial coax cable as a pulse-forming line. For this investigation, a system capable of considerably higher voltages and employing simpler spark gap operation was desired. Such a system has been developed which uses a design concept based on the statistical time lag preceding electrical breakdown. The system also employs large coaxial geometry so that extremely high operating voltage may be used and at the same time the discontinuities of the spark gap are minimized.

The basic apparatus consists of two gas-discharge switches, a "slow" switch and a "fast" switch, a test gap with Rogowski electrodes, and a pulse-forming coax line. Figure 1 is a schematic diagram of the device. The coaxial transmission line is constructed from polished aluminum pipe. The outer conductor has a 4.0 inch I.D and the inner conductor has a 1.0 inch O.D. This geometry gives a characteristic impedance of 83.3 ohms. The pulse-forming section is twelve feet long

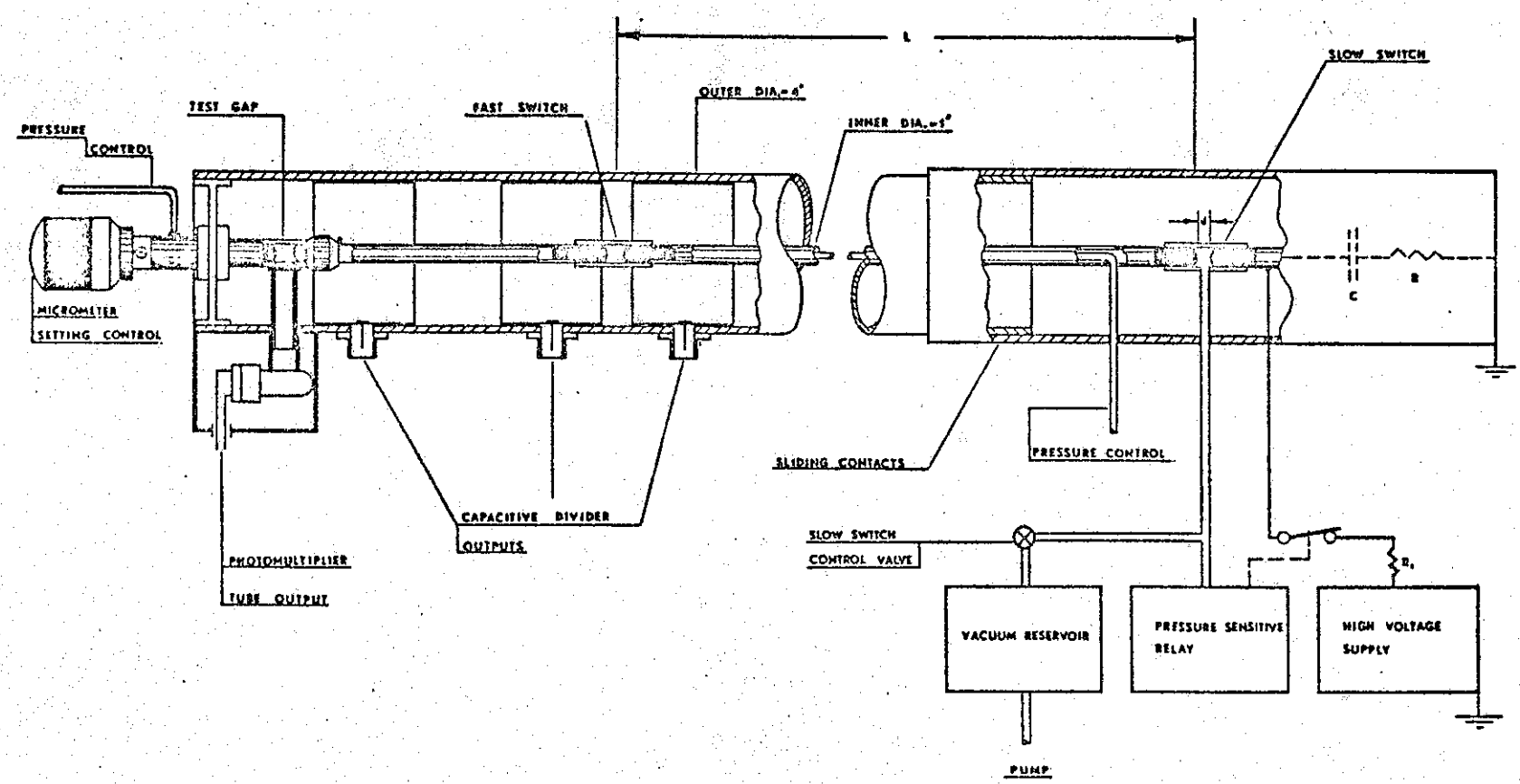

FIGURE 1

Schematic Diagram of the Experimental Apparatus

and generates a pulse approximately 24 nanoseconds wide. The large geometry was selected for three reasons:

1. The large separation between the inner and outer conductor permits the use of very high voltages.
2. The task of inserting instrumentation is simplified.
3. The gap electrodes become more nearly an integral part of the device. Special electrode sections (required when standard coax is used) which adversely affect pulse shape are eliminated.

The gas switches and the test gap are enclosed in pressure chambers. The pressure chambers for the "fast" switch and the test gap conform with the geometry of the inner conductor. The number of dielectric supports for the inner conductor has been minimized and all metallic protrusions inside the pipe are eliminated.

The slow switch charges the pulse-forming line. After the source capacitor is charged to the operating voltage, the valve controlling pressure in the slow switch chamber is opened. This causes a rapid drop in pressure in the slow switch chamber. At the same time it operates a pressure-sensitive relay which disconnects the source capacitor from the high voltage supply. This assures single-shot operation. When the pressure reaches the breakdown value, the slow switch closes and the source capacitor begins to charge the main line. The rate of charging is a function of the rate of close of the slow switch, the damping resistor, R, and the capacity of the pulse-forming line. These parameters are adjusted to assure that the time required to charge the

line is shorter than the statistical time lag of the fast switch. This charging time is usually 100 ns to 200 ns. The statistical time lag of the fast switch varies from 1.0 to 5.0 μ seconds.

When the line is charged, the voltage drop across the fast switch is almost equal to the voltage set on the source capacitor. The final value of the electric field in the test gap is determined by this voltage level and by the gap spacing. The fast switch will not break down, however, until an electron appears in the gap. When the discharge-initiating electron does appear, the breakdown begins immediately.

The fast switch rise time is a function of the electric field, the type of gas, and the gas pressure. The rise-time control is accomplished by adjusting the pressure in the fast switch vacuum chamber. It was found that an E/P ratio of 500 would result in a rise time of 2 to 3 nanoseconds. For sub-nanosecond rise times the ratio was increased to 1,000. Nitrogen gas was used in the fast switch and the pressure controlled by pumping the vacuum chamber through the hollow center conductor. This pumping technique eliminated the possibility of any discontinuity caused by pumping lines protruding directly into the coaxial line. The high-voltage, fast-rise-time pulse generated by the fast switch is applied to the test gap electrode. This gap is used to study the breakdown phenomena.

B. Instrumentation

1. Voltage Divider

The instrumentation used to measure the voltage pulse applied to the test gap was a transmission line divider similar to that used by Fletcher[5]. The dielectric was

constructed from .001" thick mylar sheets. This thickness provided a voltage division of 2100:1. One side of the sheet was coated with a highly conducting silver paint which served as the inner conductor of the transmission line divider. The sheet was cut to the exact size and then inserted inside the outer conductor of the apparatus. The divider section was made 2 feet long and the connectors were separated by 18". One connector was located near the fast switch and the other near the test gap.

There was concern that the transmission line divider would distort the pulse shape. To test this, several dividers of greatly differing lengths were tried. The signals from these dividers were all identical. Based on this result, it was assumed that pulse shape was not observably affected by the divider. The divider shown in Figure 2 was settled upon as the final design, since it was much easier to construct and install.

The signal from the capacity divider was sent directly to the deflection system of a Tektronix Model 519 oscilloscope which had a rise-time capability of 0.3 nanoseconds. Three dividers were installed so that the characteristics of the slow switch, fast switch, and test gap could be conveniently observed. A typical oscilloscope trace showing the pulse

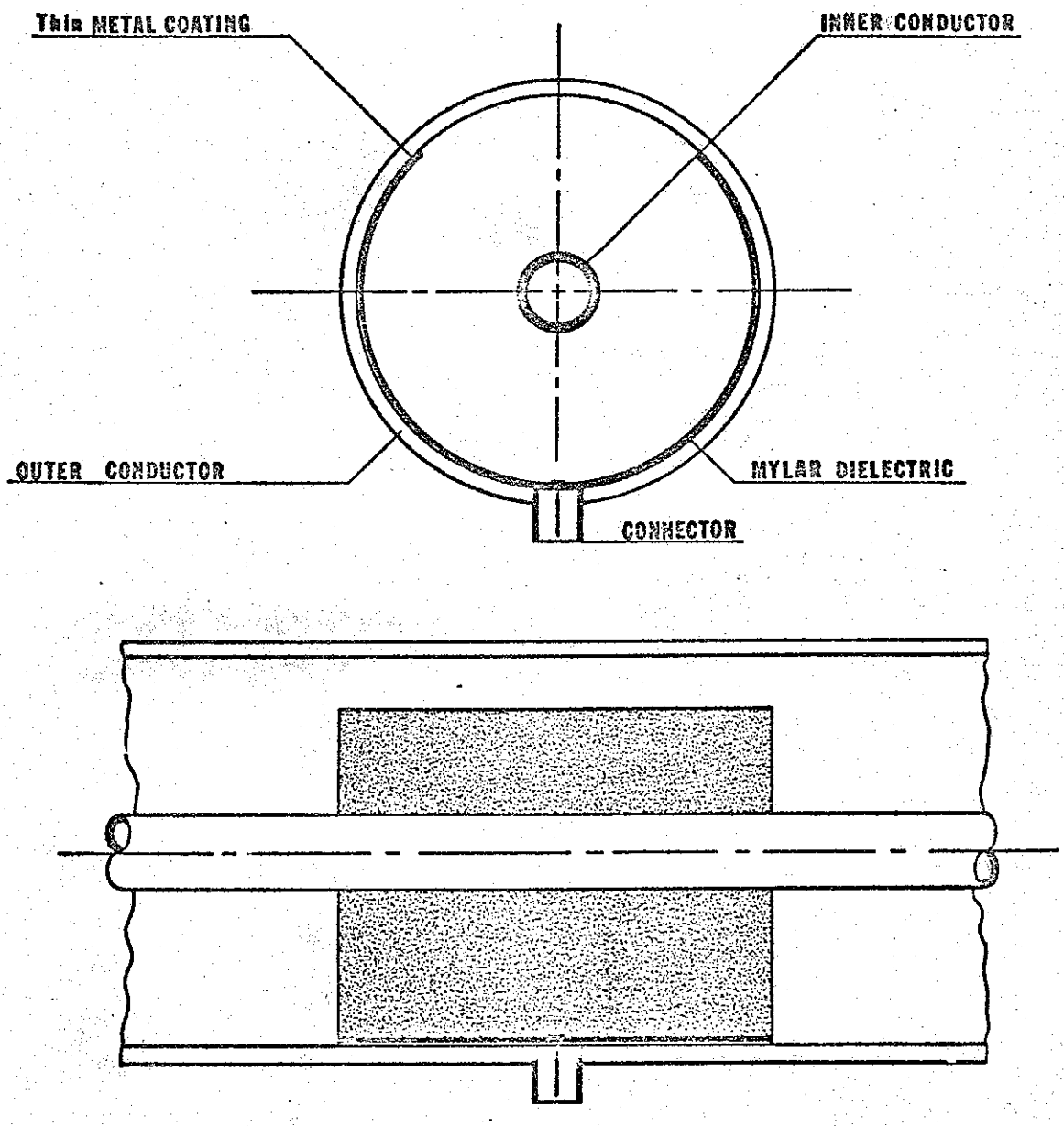

FIGURE 2

Distributed Capacity Divider

shape is shown in Figure 3.

2. Photo-Multiplier System

Instrumentation to observe the light output during gap breakdown was also added to the equipment. This instrumentation is shown in Figure 4. An RCA 1P28 photomultiplier tube was used for light detection.

It was found that a completely shielded power supply was required to eliminate the noise pickup. The supply used consisted of four 300-volt dry cell batteries mounted inside the metal light shield which surrounded the photo-multiplier system. The photo-multiplier tube itself was also enclosed inside a separate metal shield which had a slot cut in it to expose the photocathode. This shield was grounded to the outer conductor of the coaxial line. Figure 4 illustrates the shielding arrangement.

The circuitry required by the photomultiplier was designed to minimize stray inductance and capacitance. The output of this system was connected directly to the 519 scope. A typical oscilloscope trace of the signal from the photomultiplier is shown in Figure 5.

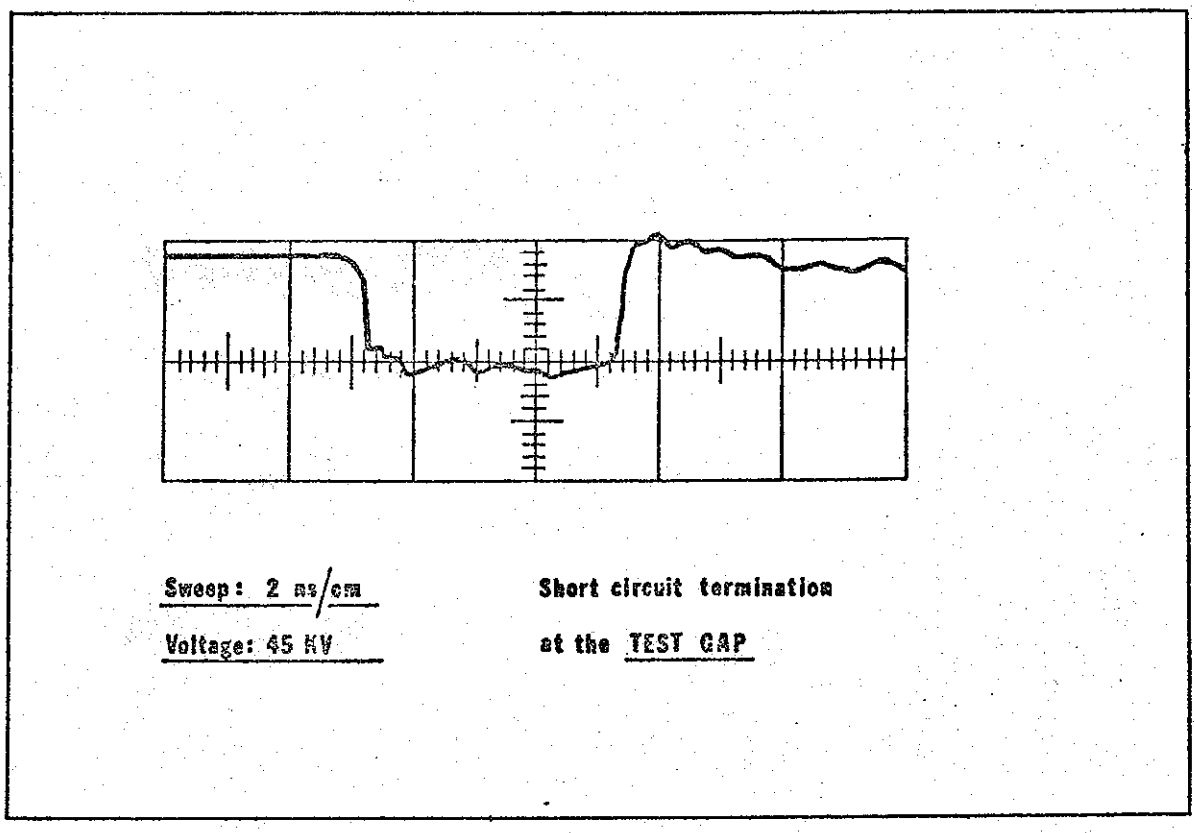

FIGURE 3

A Typical Output Signal from the Fast Switch (Original Oscillogram Transmitted to W. C. Quinn, RADC, in a Separate Communication)

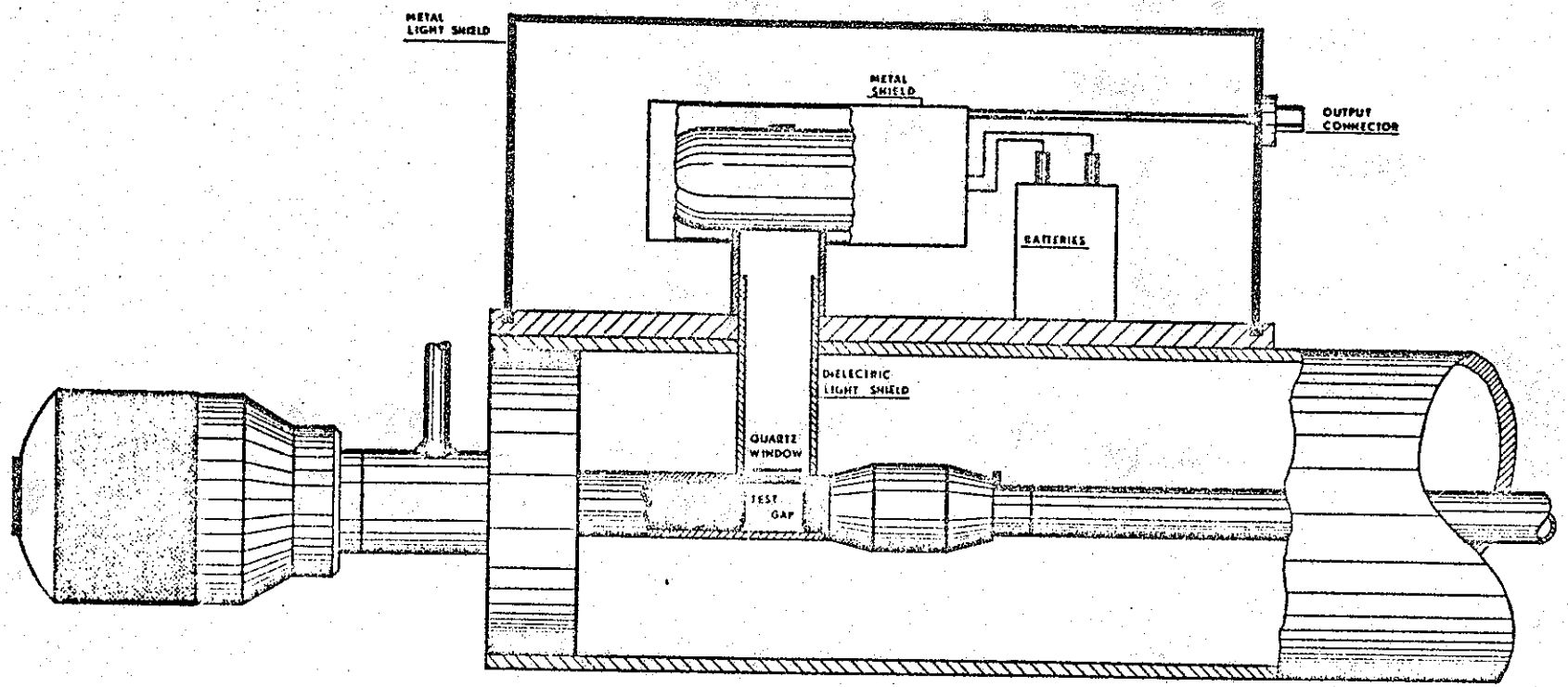

FIGURE 4

Shielding Arrangement for the Photomultiplier System

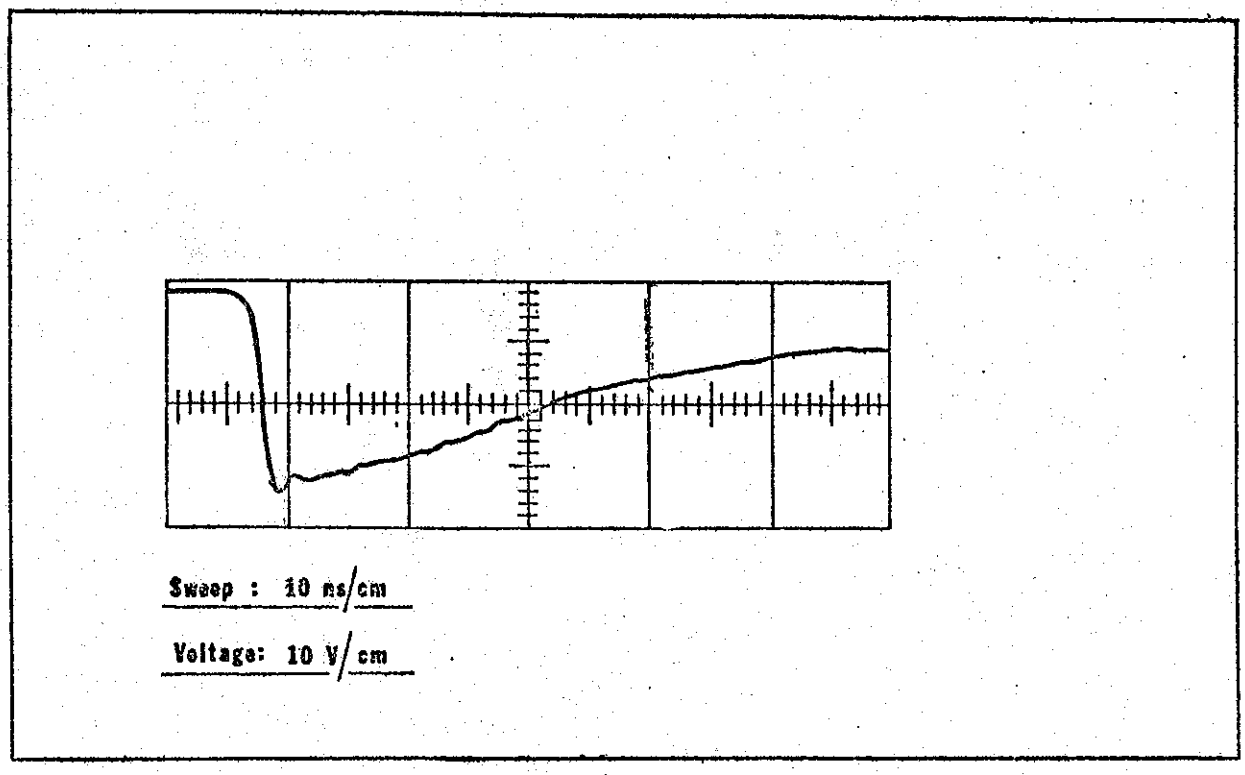

FIGURE 4

A Typical Output Signal from the Photomultiplier

SECTION III

EXPERIMENTAL PROCEDURES AND TECHNIQUES

Experimental Procedures

The technique used to obtain the statistical time lag data was straightforward and fairly fast. The procedure consisted of two parts:

1. Preliminary Adjustments

   a. The operating level of the experiment was set by adjusting the source capacitor voltage. Once this voltage is fixed the voltage level at the test gap may be calculated.

   b. The test gap spacing was adjusted by means of the micrometer setting control to give the desired electric field in the test gap.

   c. The pressures in both the fast switch and the test gap were independently set to give the desired E/P ratio.

   d. The 519 oscilloscope probe was connected to the output of the capacitive divider nearest to the test gap and the scope was set to internal trigger.

2. Time Lag Measurements

   a. When the preliminary adjustments were completed, the slow switch pressure control valve was opened, causing the slow switch to break down. This charged the pulse-forming line and applied high voltage to the fast switch. The statistical delay associated with the fast switch was adjusted by the choice of gap

spacing and choice of electrode materials to be much greater than the time required to charge the line.

b. After this delay, the fast switch operates and a rectangular voltage pulse of amplitude half the line voltage propagates toward the test gap electrode. This pulse is detected by the capacitive divider instrumentation and displayed on the oscilloscope. When the pulse reaches the test gap electrode it is reflected back and the reflected pulse also appears on the scope trace. Figure 6 shows a typical trace used in measuring a single statistical time delay. The small step at the beginning represents the time delay associated with the pulse traveling from the capacitive divider to the gap electrode and back.

c. The voltage applied to the test gap remains constant until a free electron is emitted from the test gap cathode. This free electron causes the voltage across the gap to collapse sharply since the E/P ratio is adjusted so that the formative time is much less than a nanosecond. This causes the observed voltage amplitude to drop to zero. The length of time that the voltage remains constant is the statistical lag, indicated by t_s in Figure 6. The scope sweep speed is set so that the voltage collapse can be observed.

d. The time lag, t_s, is observed visually on the scope for each shot and recorded. The process is repeated until 1,000 shots for each electrode are obtained. The electrode is then repolished, the

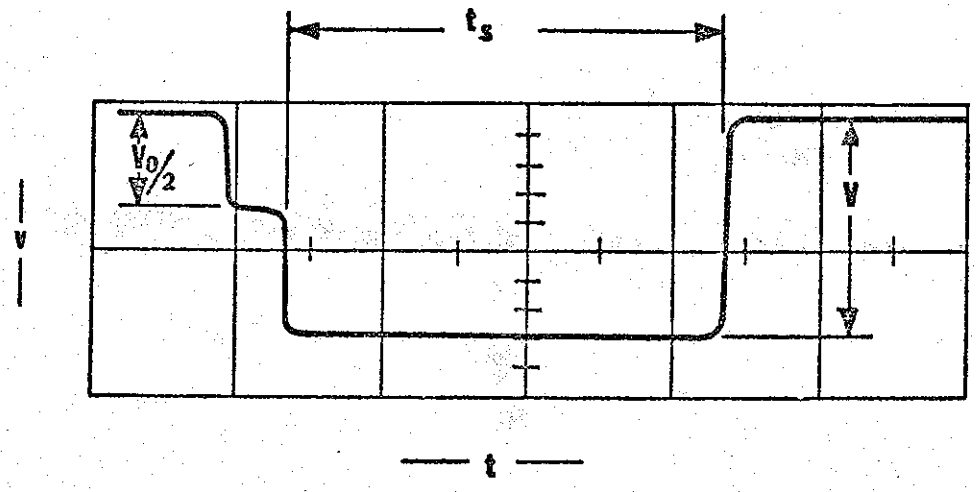

FIGURE 6

Typical Pulse For Measuring The Statistical Lag (t_s)

electric field is readjusted, and the entire procedure is repeated. The electric field settings were 100, 200, and 300 kilovolts per centimeter. At these values statistical time lags associated with field strengths as high as 10 E_s were observed with the 519 oscilloscope. Five different metal electrodes were selected. These were:

(1) Brass

(2) Bronze

(3) Steel

(4) Aluminum

(5) Silver-plated bronze

3. Experimental Conditions

To perform valid measurements of the average statistical time lag, the following conditions should be satisfied:

a. The electric field must be applied in the form of a step-function pulse with a rise time short compared to the average statistical time lag.

b. The formative time should be short compared to the average statistical time lag.

c. The electric field must be greater than 1.25 E_s.

d. The macroscopic field in the gap must be uniform.

e. No ionizing radiation such as ultraviolet or X-rays should be admitted to the test gap.

f. The cathode electron emission should be constant during the measurements.

Using the apparatus described in Section III it was possible to satisfy the first five conditions listed. The sixth condition was not met in general, since cathode electron emission is function of electrode preparation and treatment. These are discussed below.

4. Cathode Preparation

The emission rate from the cathode was found to be fairly constant only after it was completely "conditioned" or had a heavy oxide or tarnish layer. If a polished cathode surface is subjected to repeated sparking as it is during time lag measurements, the emission starts high and gradually approaches a fixed lower level. The number of sparkings, or shots, required to produce a noticeable reduction in emission is a function of surface finish.

Because of the importance of the electrode finish, a standard technique for polishing the electrodes was used. The polishing procedure which gave best results was:

a. Initial polishing with crocus cloth to remove large surface irregularities.

b. Intermediate polishing with 400 ALUNDUM powder to remove the scratches made during first stage.

c. Final polishing with jewelers' rouge and a polishing wheel to obtain a mirror finish.

Using this three-stage procedure insured that the

electrode surface finish was the same for each set of statistical measurements and that major surface roughness, microscopic splinters, and similar surface features were eliminated. Microscopic scratches did remain, however, and were removed only by conditioning.

SECTION IV

EXPERIMENTAL RESULTS

A. Statistical Time Lag Measurements

The curves shown in Figures 7 through 20 are plots of emission as a function of the number of breakdowns for a constant electric field. These curves represent the emission associated with the conditioning of the electrode surface. The value of emission for a given number of breakdowns was computed from equation (1-3) using 50 time lag data points which preceded the given number of breakdowns. For example, the point at n = 700 was computed using the data between 650 and 700. Fifty data points were selected since this number was small enough to permit the assumption of constant emission and at the same time large enough to have some statistical meaning.

As can be seen from the curves, the emission is somewhat erratic with an overall characteristic decreasing with the number of breakdowns. Some of the variation is due to occasional electrode pitting as the electrode approaches the conditioned state.

The statistical data for the aluminum electrode was very erratic and was taken several times. It was found that the statistical times for aluminum at 200 and 300 kv/cm were almost the same and for this reason only the data for 200 kv/cm is presented.

It is also seen from the data that the least active metal was steel. This result may be due to the fact that steel is much harder than the other metals tested.

Table I presents a summary of the emission of the various metal averaged over shots 700-1,000.

TABLE I

ELECTRON SURFACE EMISSION IN ELECTRONS PER SECOND

Electric Field (kv/cm)	Brass	Bronze	Silver	Aluminum	Steel
100	1.3×10^4	1.4×10^4	2.2×10^6	2.4×10^6	8.3×10^2
200	3.6×10^4	1.6×10^6	1.3×10^7	1.2×10^8	1.7×10^4
300	3.2×10^6	1.7×10^8	1.4×10^8	1.2×10^8	3.5×10^5

Ranking the metals in the order of least active to most active, one obtains: (1) steel, (2) brass, (3) bronze, (4) silver, and (5) aluminum.

Although no definite conclusion can be attributed to this order, it does appear to be related to either the conductivity of the metal, with aluminum being an exception, or to the hardness of metal again with aluminum being the exception. The fact that aluminum does not fit either of these criteria could be due to its low melting point as compared to the other metals. It was also observed that the aluminum electrodes were more susceptible to spark damage than the other metals. Again, this is probably due to the low melting point of aluminum (600°C).

B. "Conditioning"

Even a polished surface has scratches and other irregularities easily observed under a microscope. A process which leads to a "conditioned" surface consists of sparking a polished electrode until

these surface irregularities are eroded away and the surface has a uniform, very fine grainy structure. This process results in a less active surface. Figure 21a is a micrograph of a bronze electrode after polishing. Figure 21c illustrates the same electrode after a large number of sparks have occurred. It is observed that the polishing marks are removed and a fine grainy structure is visible. This surface represents the conditioned state for the metal. Similar results have been observed for all of the metals. Figure 21b shows the result of electrode pitting.

C. Photo-optics

The sensitivity of photo-optics system was less than was expected, but it still was capable of detecting the light emitted from the spark in the final stages of development. A few calculations of discharge current buildup for several values of E/P illustrate the speed at which the electron growth rate proceeds near the final stages. For purposes of the calculations, a uniform electric field of 40 kv/cm was used. A simple exponential current buildup was assumed with a time constant τ determined by ionization frequency data.

Table II shows the time, t_1, required for the discharge current to reach 1.0 ampere and the time, t_2, required to reach the full breakdown value of 482 amperes.

TABLE II

E/P	τ	t_2	t_1	$t_2 - t_1$
52.5	4.55×10^{-10}	21.9 ns	19.8 ns	2.1 ns
100	10^{-10}	4.83 ns	4.35 ns	0.48 ns
500	1.08×10^{-11}	0.526 ns	0.473 ns	0.05 ns
1,000	7.52×10^{-12}	0.367 ns	0.33 ns	0.037 ns

From Table II it can be seen that if only the rise of current from t_1 to t_2 is observed, a rise time resolution of about .03 nanoseconds would be required to detect differences in the final stages of the spark growth. The rise time capability of the photomultiplier was about 2.5 to 3 nanoseconds as can be seen from Figure 5, Section III. Because of this limitation, growth rate measurements were not attempted.

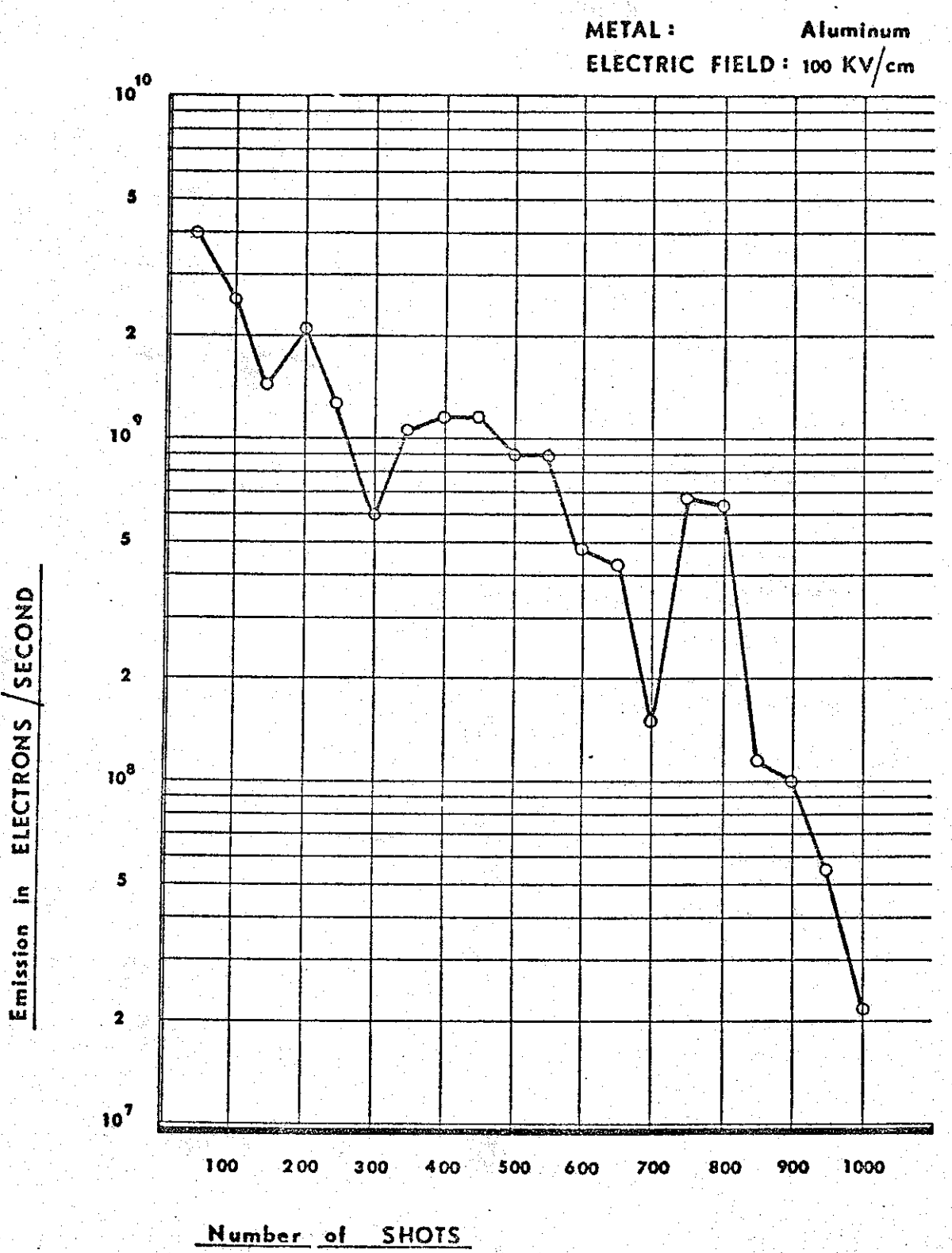

FIGURE 7

Emission Data for Aluminum at 100 KV/cm

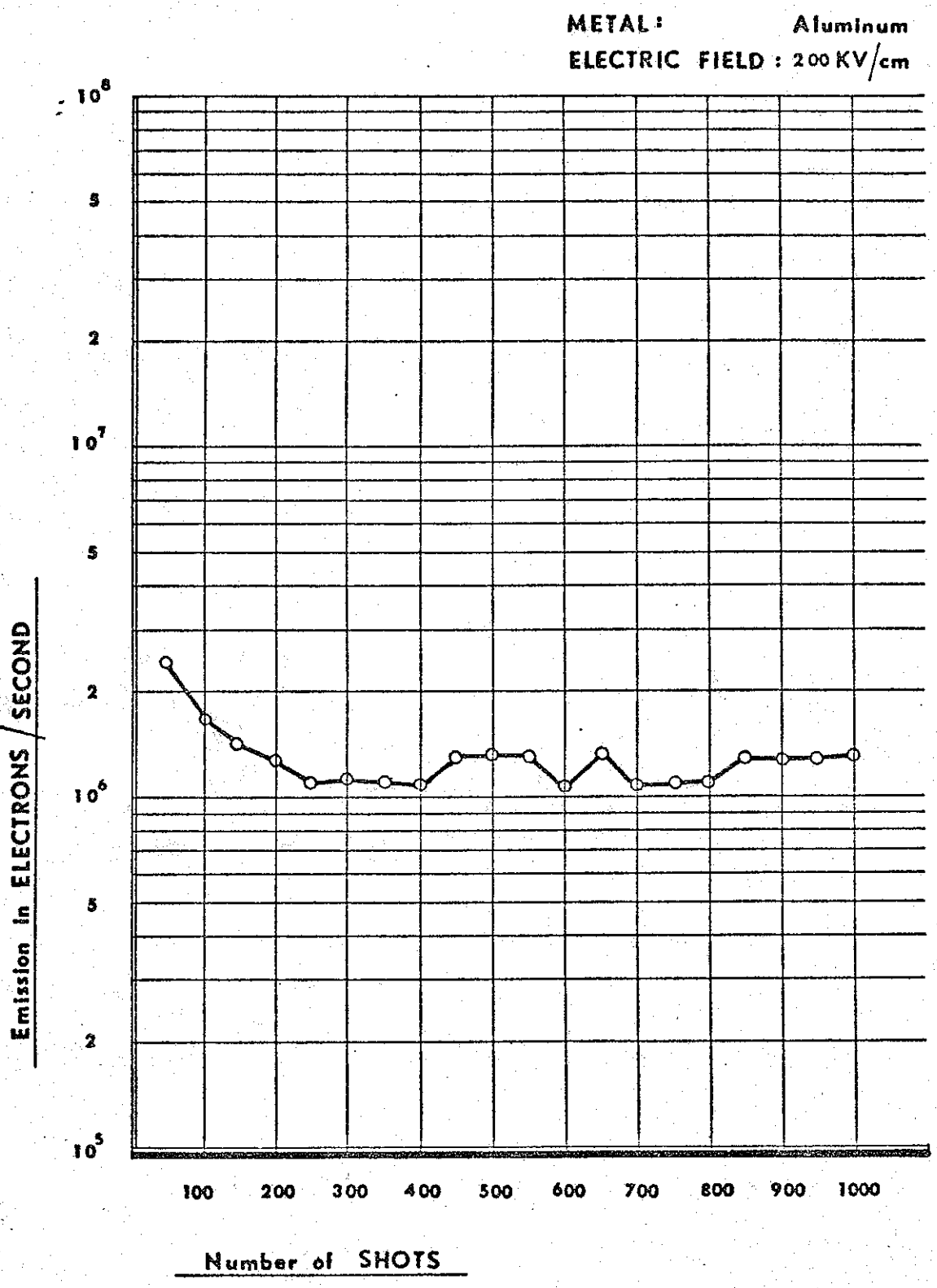

FIGURE 8

Emission Data for Aluminum at 200 KV/cm

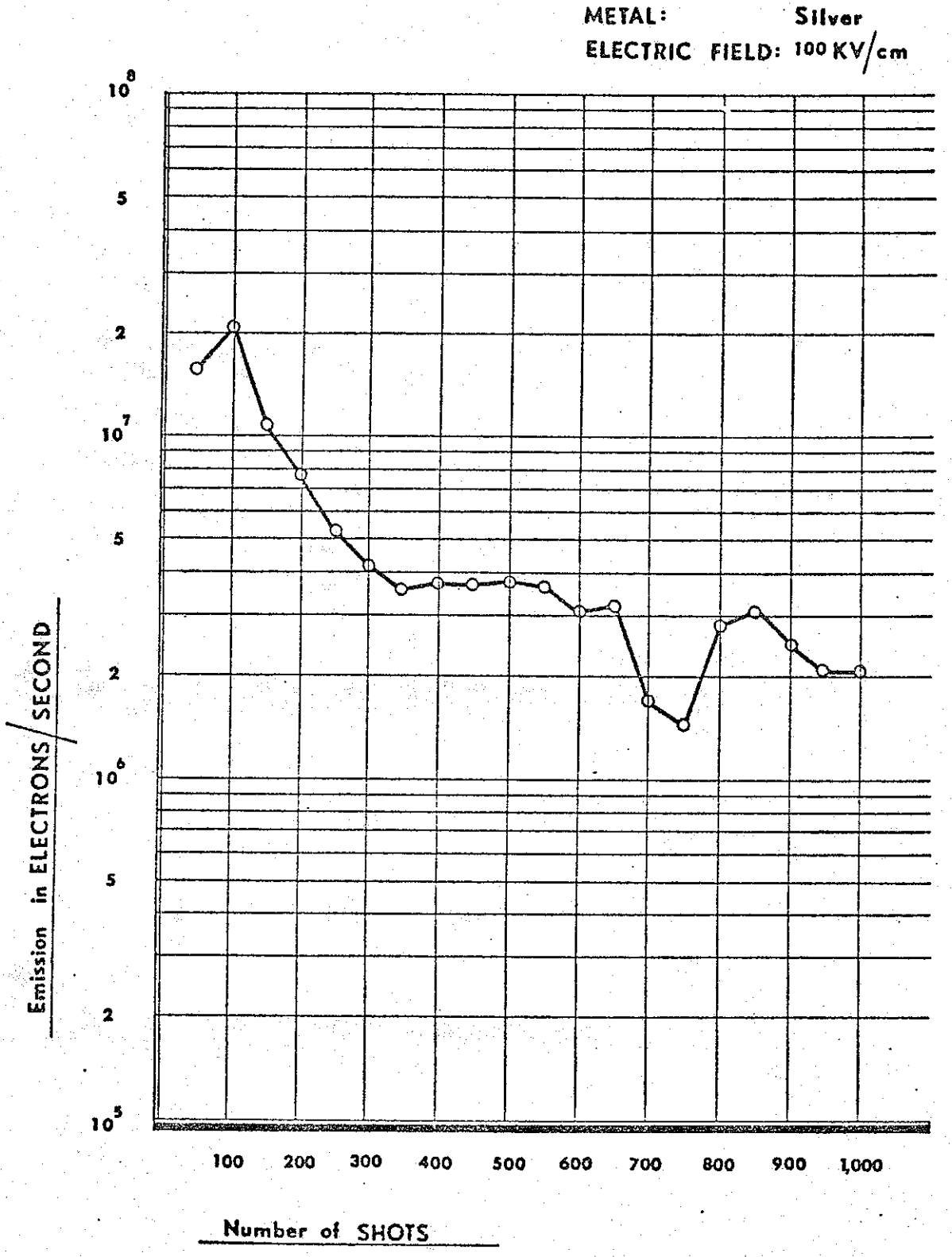

FIGURE 9
Emission Data for Silver at 100 KV/cm

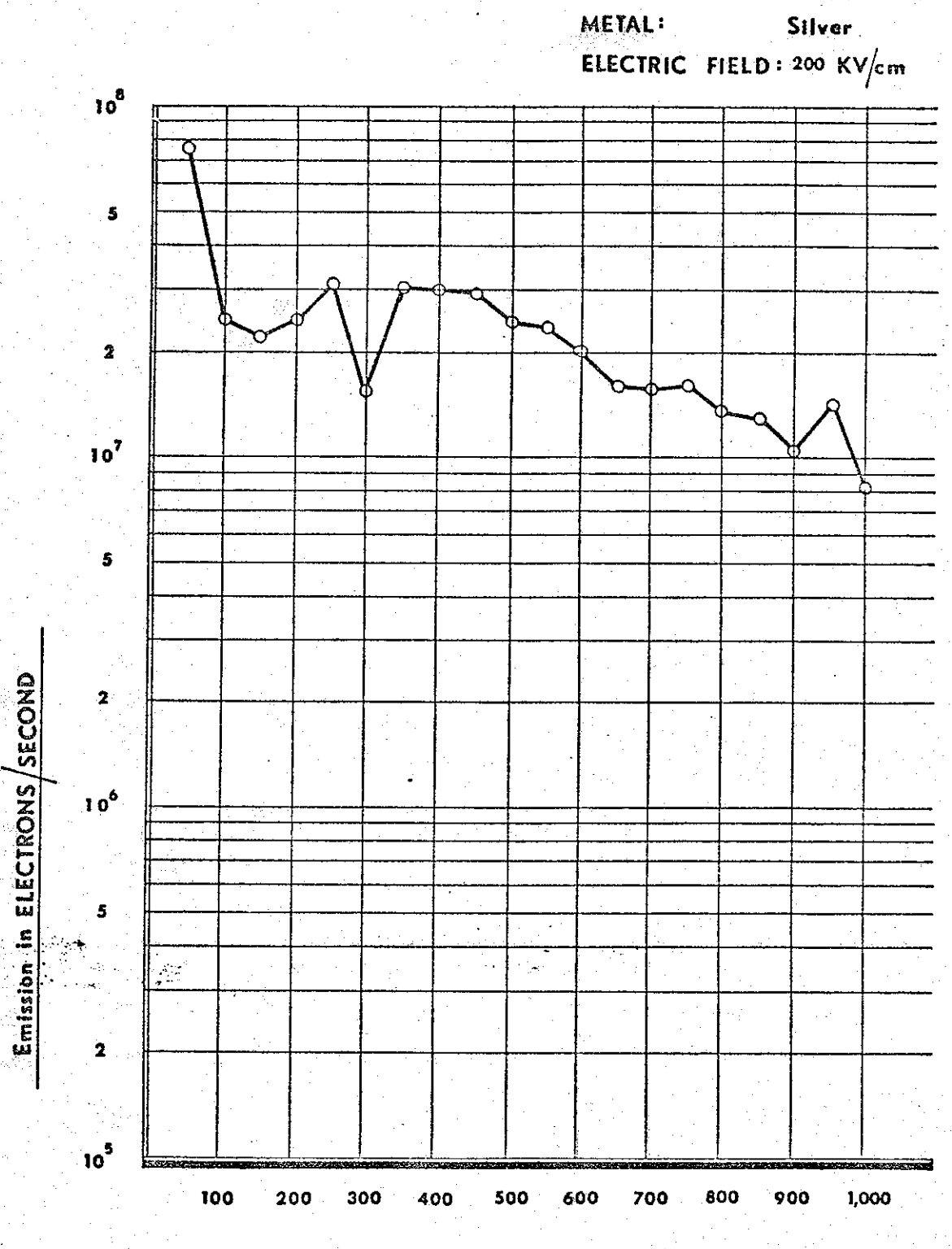

FIGURE 10

Emission Data for Silver at 200 KV/cm

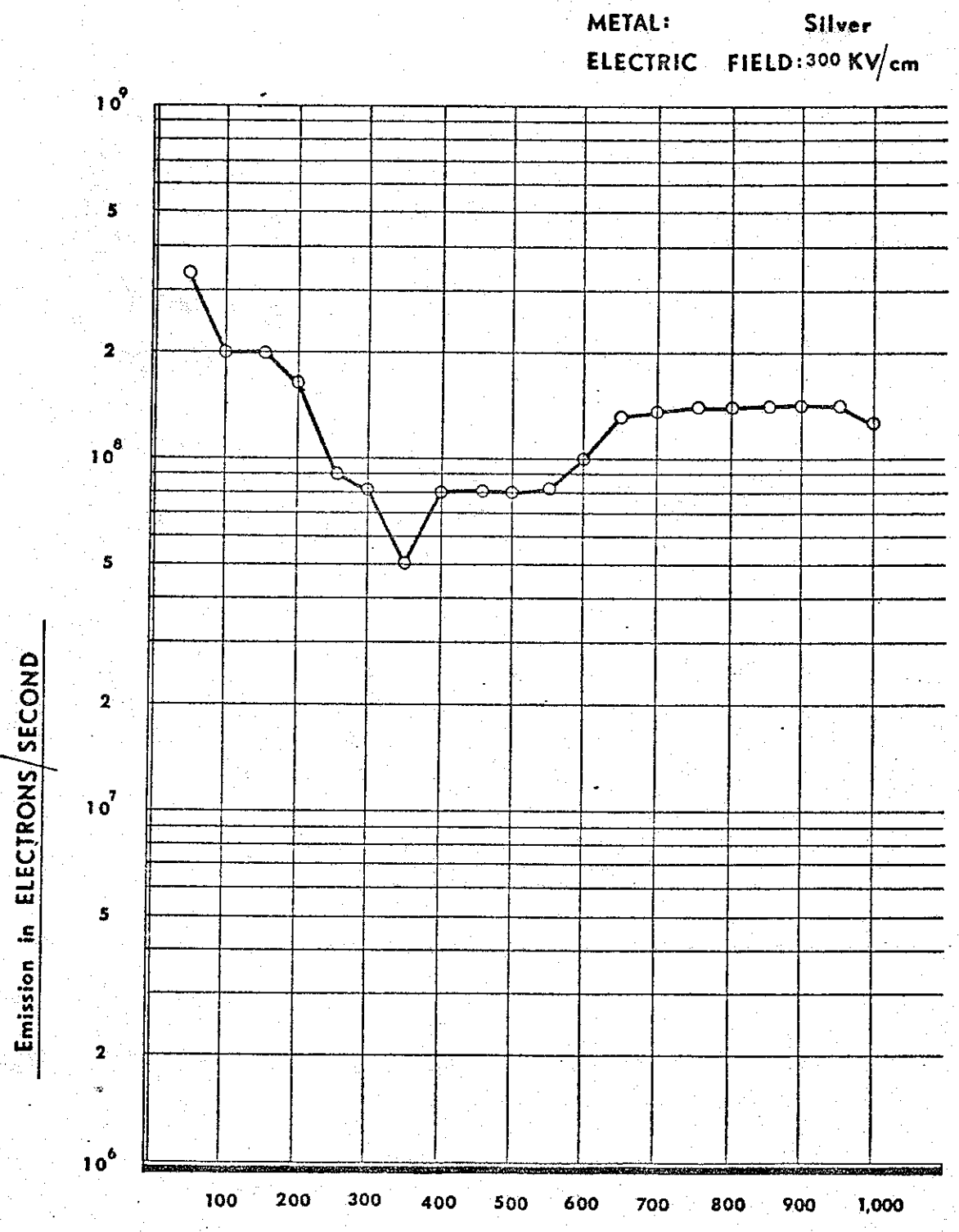

FIGURE 11

Emission Data for Silver at 300 KV/cm

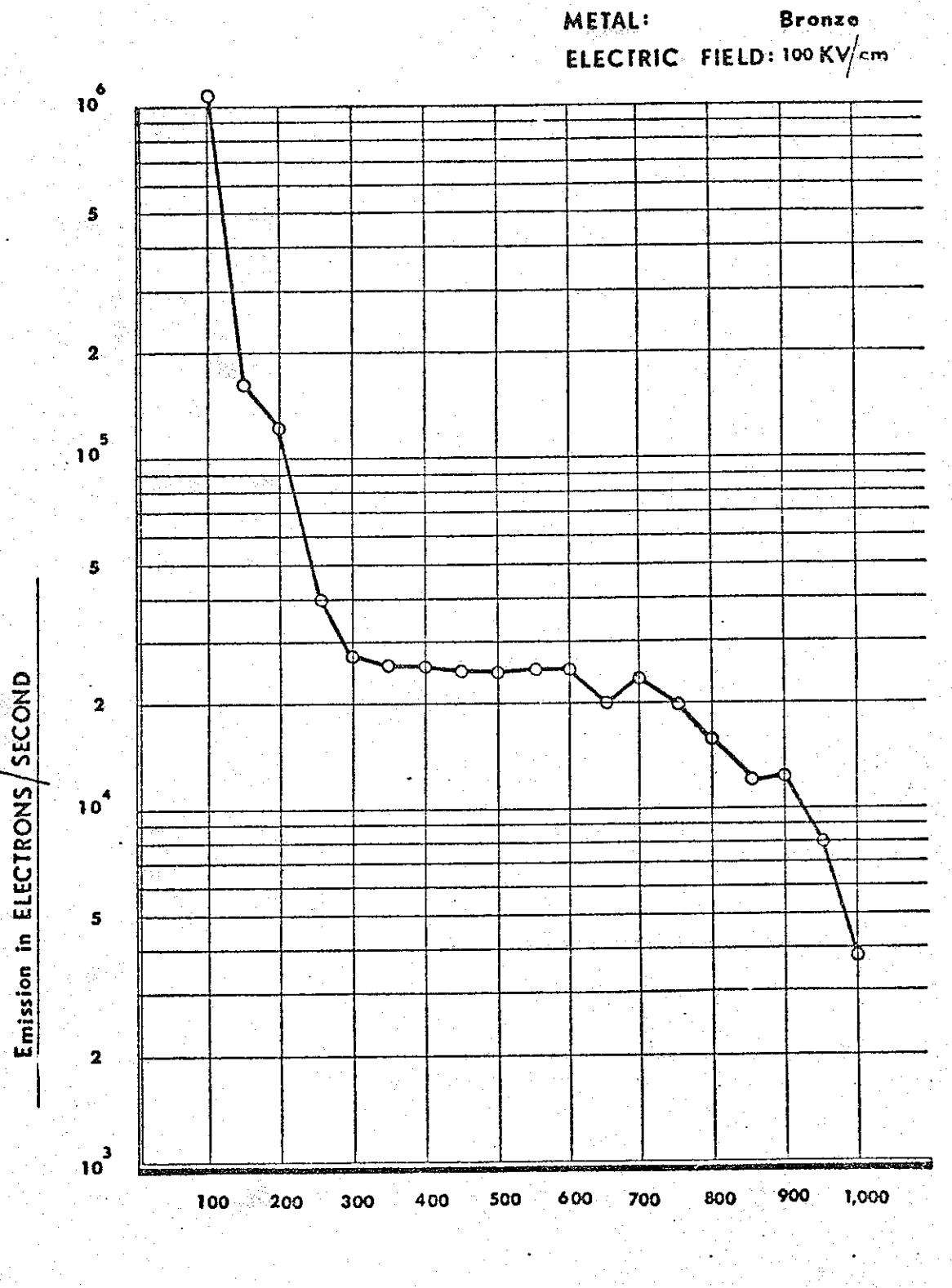

FIGURE 12

Emission Data for Bronze at 100 KV/cm

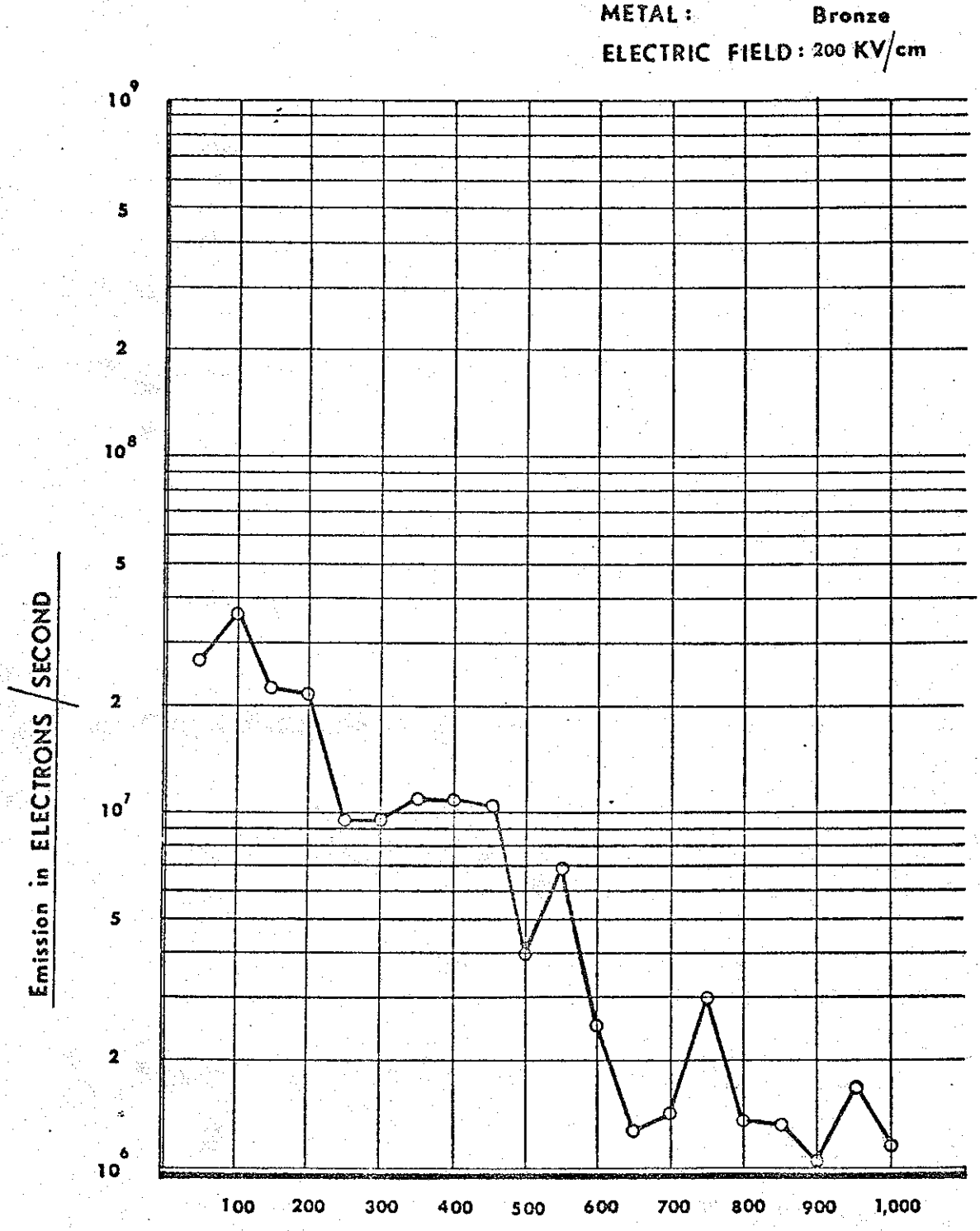

FIGURE 13

Emission Data for Bronze at 200 KV/cm

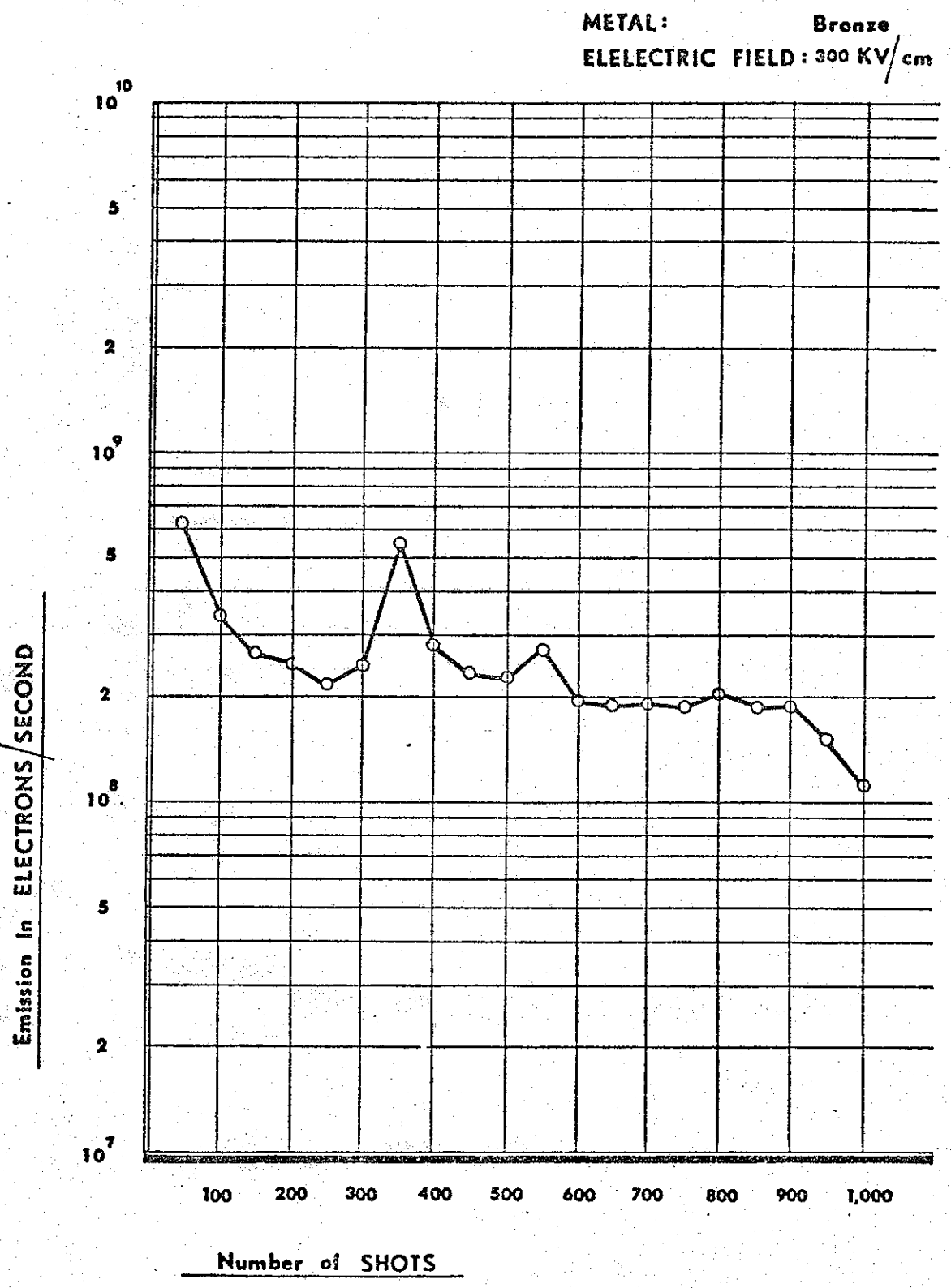

FIGURE 14

Emission Data for Bronze at 300 KV/cm

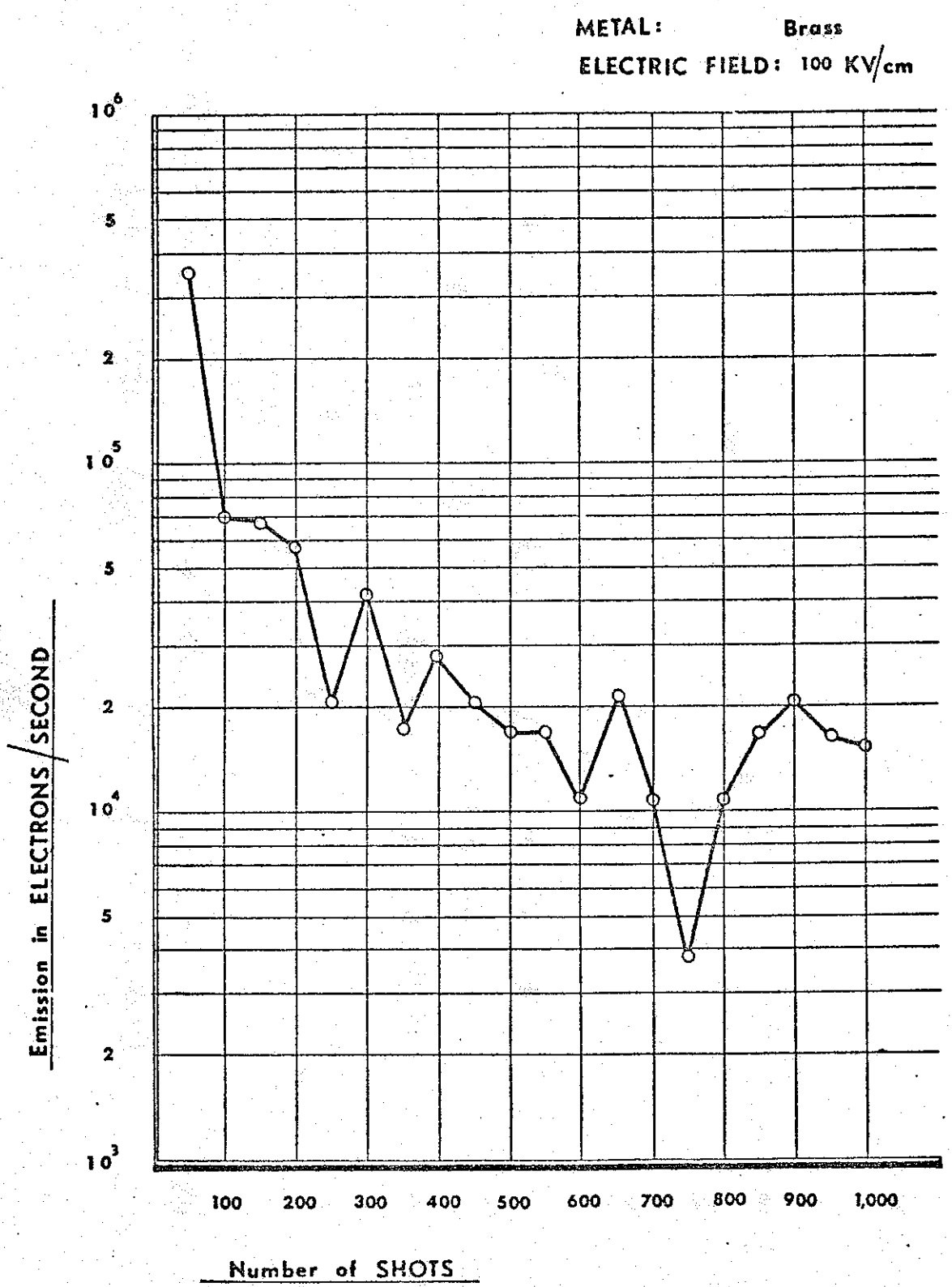

FIGURE 15

Emission Data for Brass at 100 KV/cm

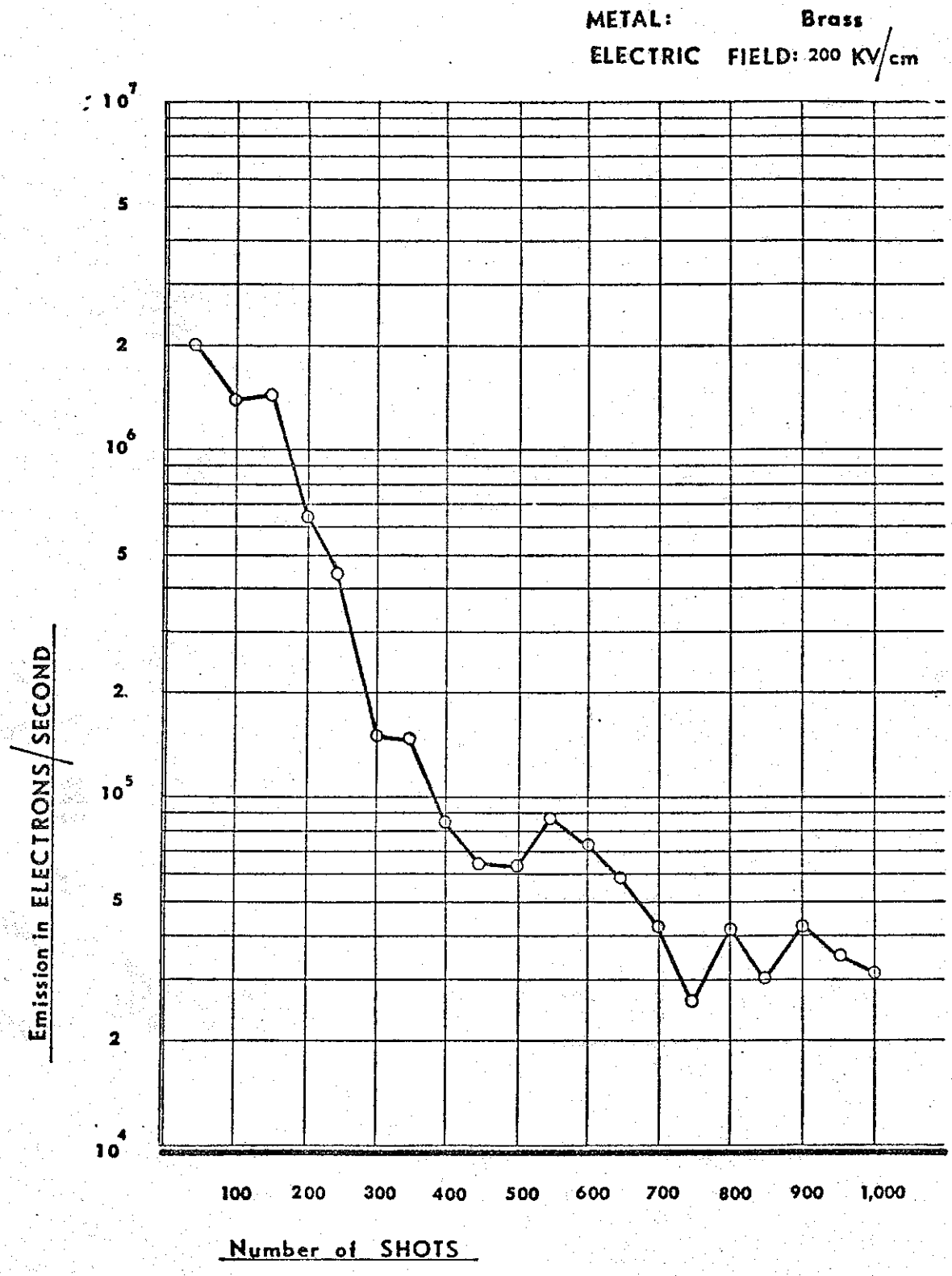

FIGURE 16

Emission Data for Brass at 200 KV/cm

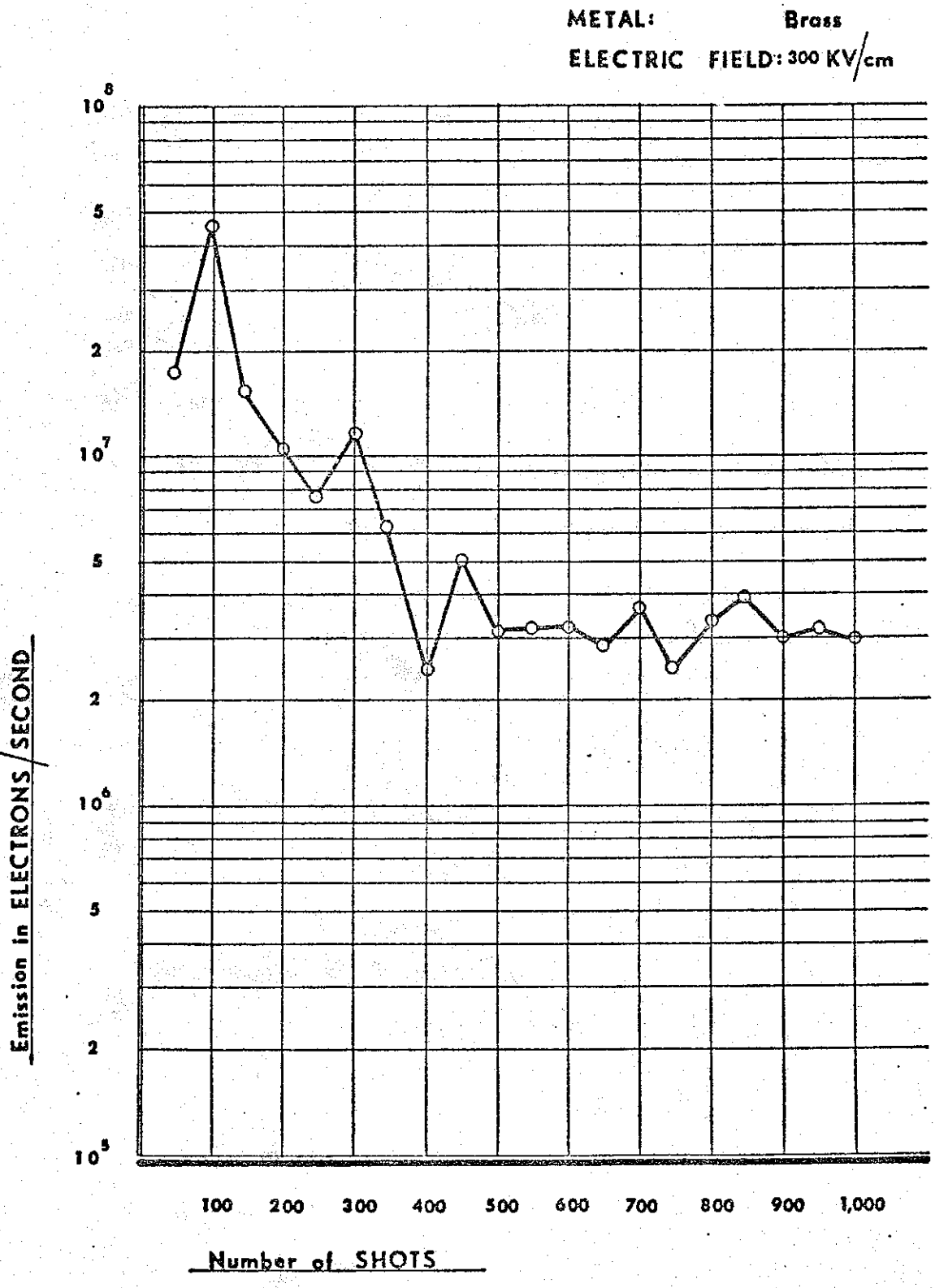

FIGURE 17

Emission Data for Brass at 300 KV/cm

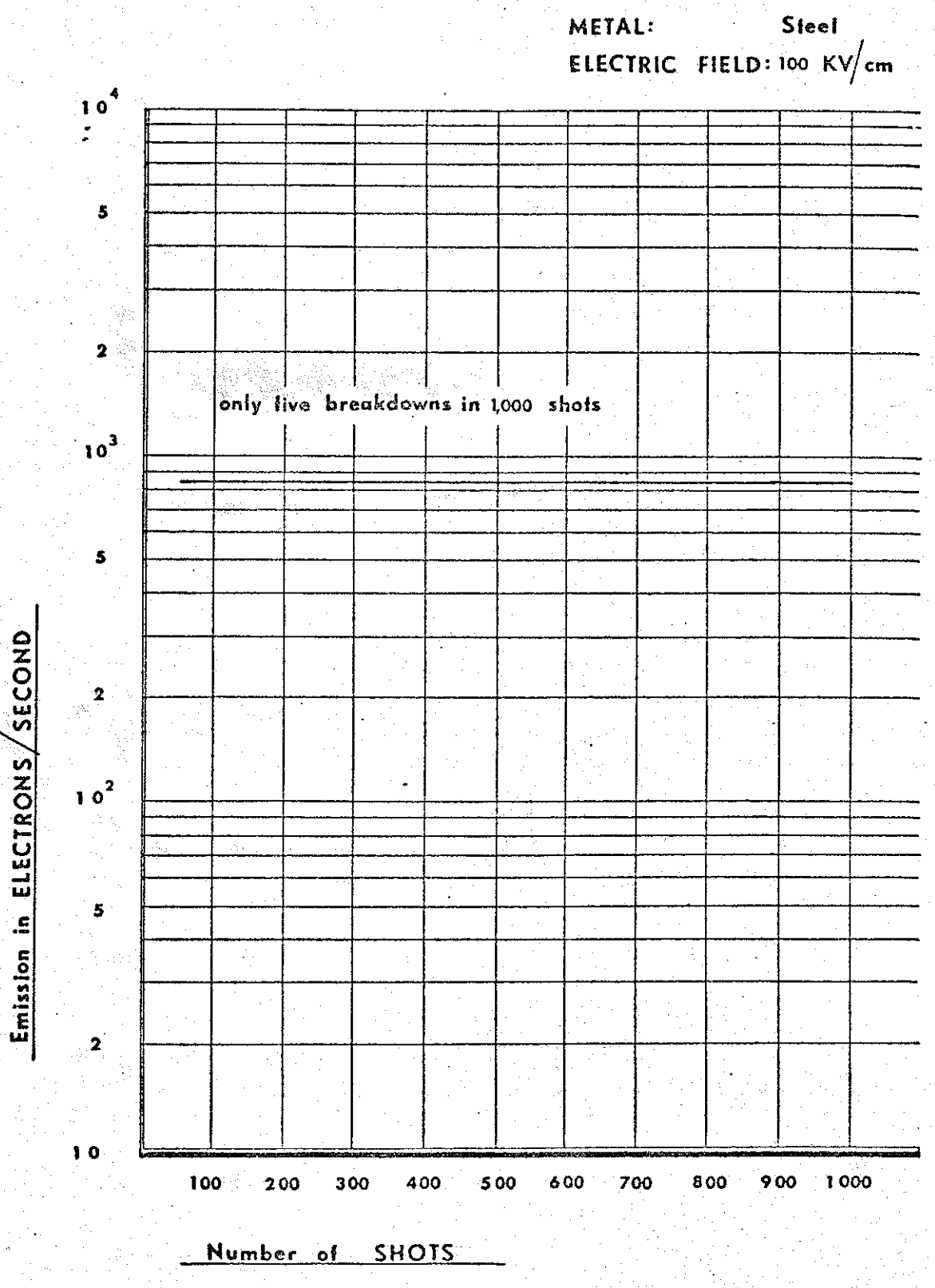

FIGURE 18

Emission Data for Steel at 100 KV/cm

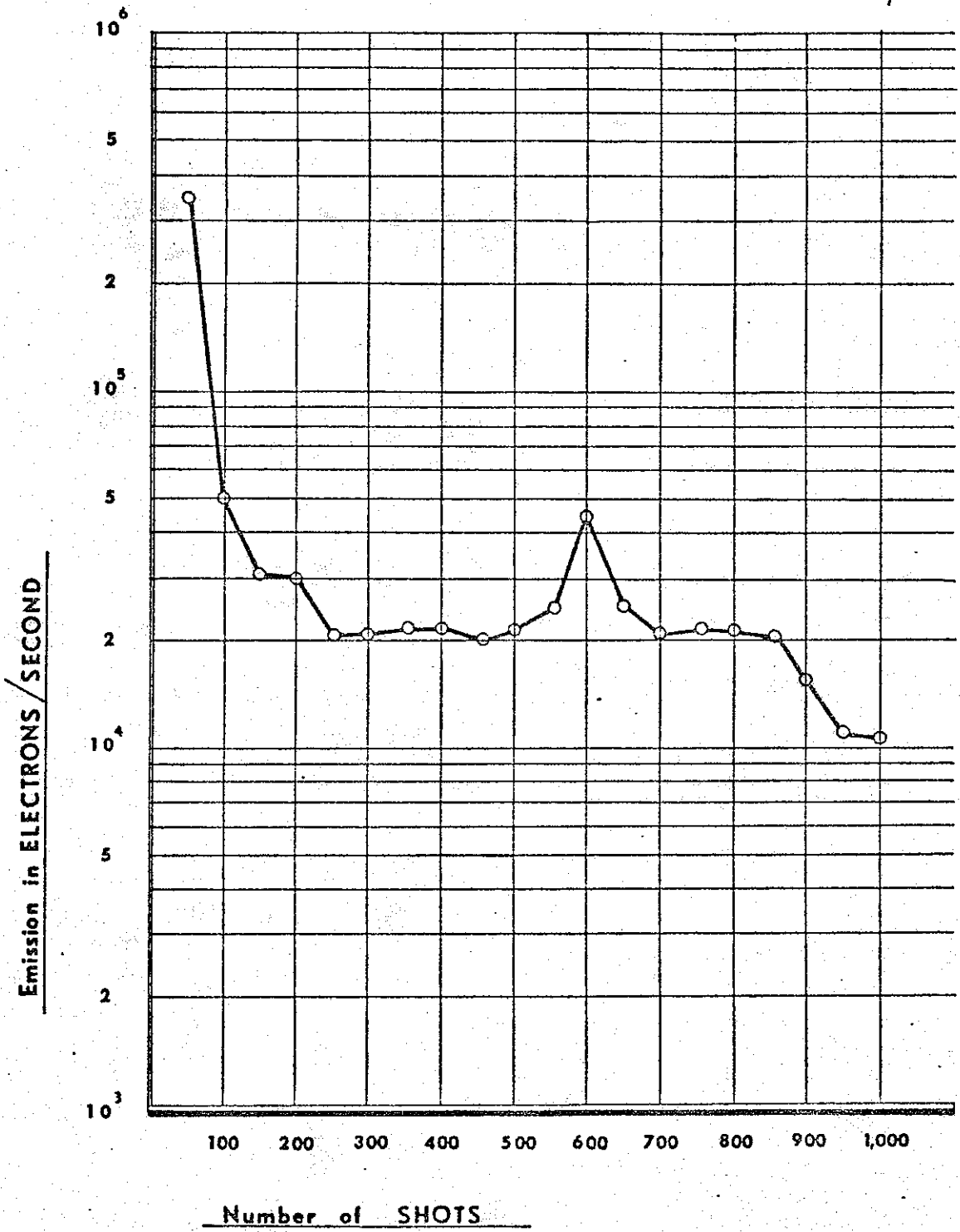

FIGURE 19

Emission Data for Steel at 200 KV/cm

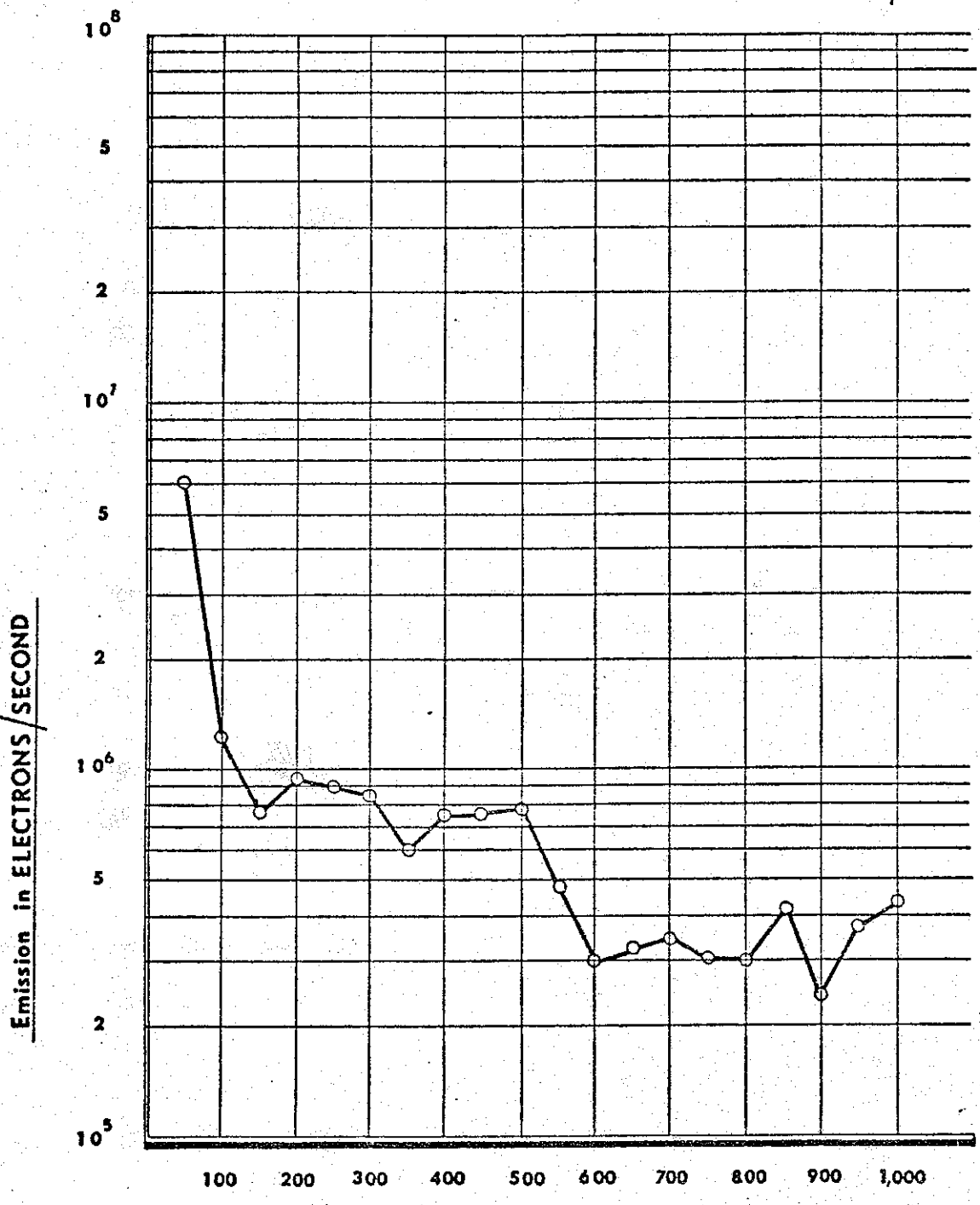

FIGURE 20

Emission Data for Steel at 300 KV/cm

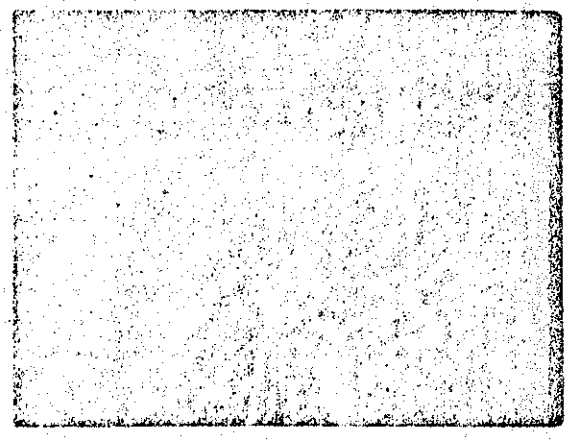

a. Polished cathode surface before spark gap operation

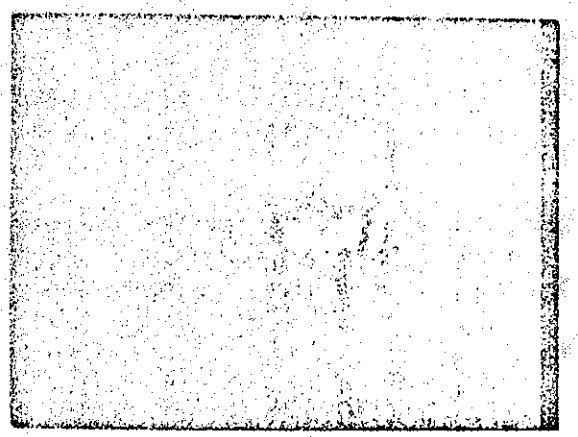

b. Pitted cathode surface

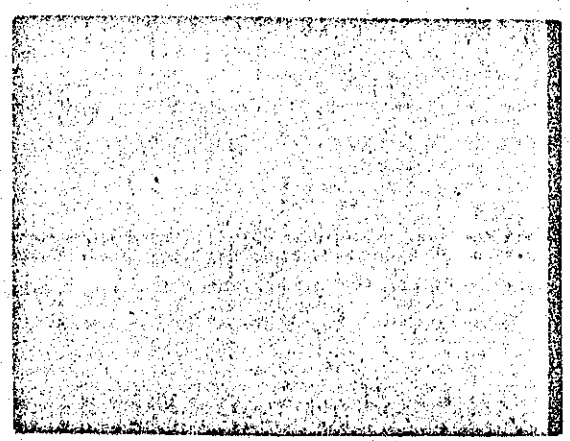

c. Grainy surface of "conditioned" cathode after 1,000 spark gap operations

FIGURE 21
PHOTOMICROGRAPHS (200X) of CATHODE SURFACE CHARACTERISTICS

SECTION V

ATMOSPHERIC BREAKDOWN

A. Introduction

Work being conducted at Rome Air Development Center has shown that at power levels expected in future systems, pulse widths and peak field strengths may be sufficient to lead to breakdown in the atmosphere. As in the case of breakdown within wave guides and near antennas, this breakdown will occur only when free electrons are present. This section will discuss the agencies which produce free electrons in the atmosphere and develop a simple statistical model of breakdown in free space.

B. Atmospheric Production of Free Electrons

For altitudes below fifty kilometers, the agencies mainly responsible for the forming of free electrons in air are:

1. Radiation from radioactivity in the earth and in local equipment materials.
2. Radiation from the radioactive gasses in the air itself.
3. Cosmic radiation.

The earth's crust and the materials used in construction and in equipment contain widely distributed small quantities of uranium, thorium, and other radioactive materials which emit ionizing radiation (alpha, beta, and gamma-rays) into the air. Alpha-rays penetrate only a few centimeters from their source, beta-rays penetrate up to

several meters, and gamma-rays penetrate farthest of all and are consequently the most effective in producing free electrons in the atmosphere above the earth. The ionization associated with these rays is confined to a region less than two kilometers above the surface. At the earth's surface the intensity of this radiation varies, but from data on the associated ionization[6] it is estimated that it is around 0.1 particles/cm^2-sec.

The air itself contains a number of gasses, such as radon, thoron, and their disintegration products, which are radioactive and produce ionization. These gasses diffuse from the earth and are mixed in the air by atmospheric turbulence. From ionization data the radiation due to atmospheric gasses is estimated to be 0.1 particles/cm^2-sec. It is confined generally to less than two kilometers altitude.

Cosmic radiation, whose nature and origin are still subjects of much investigation, comes into the atmosphere from extra-terrestial origins. Its most remarkable characteristic is its penetrating power, its range in air being many times greater than that of gamma radiation of radioactive substances. The characteristics of cosmic radiation will be discussed in more detail in a later section.

C. Statistical Model of Atmospheric Breakdown

In considering atmospheric breakdown in a high-power microwave beam, it will be assumed that the beam power density levels are above the breakdown threshold in all regions of interest. Three characteristic regions within the volume through which the beam energy passes will be examined:

Region 1 - Between the feed horn and the reflecting dish.

Region 2 - Between the reflecting dish and an altitude of 2 km.

Region 3 - Between 2 km and 50 km altidude.

Region I deserves separate analysis because at lower power levels the region between the horn and the dish is the only region in which power densities reach breakdown levels. Power levels are greatest at the horn and decrease rapidly as the beam approaches the dish. Regions 2 and 3 are considered separately because different sources of ionization predominate in these regions. In Region 2 the principal ionizing agency is natural radioactivity from the earth and from the gasses in the air. The effects of cosmic radiation may be neglected. In Region 3 only cosmic radiation contributes to electron production. Cosmic radiation arrives in bursts of 10^4 to 10^7 particles, whereas the ionizing radiation from natural radioactivity is due to single particles or pairs of particles which occur randomly in time and space. These differences lead to great differences in the results of statistical analyses of the breakdown in Regions 2 and 3, although the average flux levels due to natural radioactivity and to cosmic rays may be comparable.

REGION 1

As microwave energy travels from the feed-horn to the reflecting dish, it passes through a volume which is approximately conical. The base of the cone is the area of the reflecting dish. Any ionizing particle which produces electrons in this volume which are still unattached when the microwave pulse passes will initiate breakdown.

Only ionization due to natural radioactivity will be considered. It will be shown later that the effects of cosmic radiation may be neglected. From ionization data the total flux of particles due to natural radioactivity is estimated to be typically 0.2 particles/sec-cm^2, but it may reach 1.0 particles/sec-cm^2 in the presence of equipment. Most of these particles will pass through the conical volume. Therefore, to estimate the number of particles entering this volume per unit time, it is necessary only to compute the number which pass through a projected area of the cone. This area will vary according to the orientation of the plane of projection. The area of the reflecting dish A_D can be taken for the purposes of this analysis. Thus, the number of ionizing particles entering the cone per second is

$$A_D I \qquad (5\text{-}1)$$

where I is the local particle flux in particles/cm^2-sec. If τ is the time for all electrons in a burst to attach to neutral ions, any ionizing particle entering the volume during a time τ preceding the passage of the pulse will provide some free electrons to initiate a discharge. The average number of electrons, N_1, entering this volume during a time τ is then:

$$N_1 = A_D I \tau \qquad (5\text{-}2)$$

Using the Poisson formula, the probability, P_1, that a free electron

will be present when the pulse passes through Region 1 is:

$$P_1 = N_1 e^{-N_1}$$

$$= A_D I \tau e^{-A_D I \tau} \qquad (5\text{-}3)$$

Taking as typical numerical values the following:

$\tau = 10^{-7}$ sec (See reference 1, page 10)

$I = 0.5$ particles/cm^2-sec

$A_D = 10^6$ cm^2

yields

$P_1 = 0.05$

REGION 2

In this region the beam spreads laterally along the path of propagation. Beam diameter, D_B, as a function of range, R, dish diameter, D_D and beam angle, α, is given approximately as follows:

$$D_B = D_D + \alpha R \qquad (5\text{-}4)$$

where α is the beam angle. For purposes of this analysis this is more conveniently expressed as a function of altitude, H, and antenna elevation, θ, as follows:

$$D_B = D_D + \frac{\alpha H}{\sin \theta} \qquad (5\text{-}5)$$

Ionizing particles passing through the volume defined by the path of the beam energy will generate free electrons. The particles passing through any portion of the beam can be estimated by determining the number passing through the area projected by this portion on a plane parallel to the beam path. Along a differential length of beam path, dR, this projected area is as follows:

$$D_B dR \tag{5-6}$$

The total number of ionizing particles, N_2, passing through the volume defined by the beam energy path which can produce discharge-initiating electrons in Region 2 is given by

$$N_2 = \int_0^{H_2} D_B I\tau \, dR \tag{5-7}$$

where D_B is the diameter of the beam at range, R. I is the local particle flux density and H_2 is the upper altitude limit of Region 2. Here the time τ is the time required for a burst of free electrons created by an ionizing ray to decrease to zero. Although τ is a function of pressure and, therefore, also a function of altitude, it does not vary significantly from 0 to 2 km altitude.

The local flux intensity of incident particles is due to natural radioactivity of the earth and atmosphere. This intensity decreases with altitude and is negligible at 2 km. No accurate data in the altitude distribution of intensity is available. For purposes of these analyses this intensity distribution is assumed to be as follows:

$$I = I_o \left(1 - \frac{H}{H_2}\right), \quad H \leq H_2 \tag{5-8}$$

where I_o is ground level of ionization intensity. Using equations (5-5) and (5-8) in equation (5-7) and integrating yields

$$N_2 = \frac{I_o \tau}{\sin\theta} \left(\frac{D_D H_2}{2} + \frac{\alpha H_2^2}{6 \sin\theta}\right) \tag{5-9}$$

For a typical case the following values may be used:

$$Io = 0.2 \text{ particles/cm}^2\text{-sec}$$

$$\tau = 10^{-7} \text{ sec}$$

$$H_2 = 2 \times 10^5 \text{ cm}$$

$$\sin\theta = 0.5$$

$$D_D = 10^3 \text{ cm}$$

$$\alpha = 10^{-2}$$

These yield

$$N_2 \cong 9$$

It is easily shown that the probability, P_2, that one or more ionizing events occurs is 0.998.

REGION 3

Between 2 km and 50 km the principal source of ionizing radiation is cosmic radiation. Primary cosmic radiation is of extra-terrestial origin and consists mainly of protons (86%) and alpha particles (13%) with energies ranging from 10^9 to 10^{20} ev.

The primary radiation interacts with the upper atmosphere producing secondary particles. These secondary particles consist mainly of mesons, electrons, and high-energy gamma rays. By

subsequent transformation these particles are multiplied into millions of particles creating an extensive shower of high-energy particles penetrating downward into the atmosphere. The showers penetrate many miles spreading laterally only ten to 100 meters. The cosmic radiation which is observed between 2 km and 50 km consists of these bursts of high-energy particles. The average number of particles in these bursts is of the order of 10^6 particles per burst.

Secondary cosmic radiation affects microwave beam transmission in a different way from natural radioactivity in the atmosphere. Natural radioactivity produces ionizing rays singly or at most in groups of two or three particles. Cosmic radiation, on the other hand, produces millions of particles within a few microseconds over an area of 10^2 to 10^4 m^2. The effect on microwave beam transmission will be quite different.

To determine the number of cosmic ray bursts which generate free electrons in the region through which the beam energy is passing, much of the previous analysis used for Region 2 is applicable. Equation 5-7 may be adapted to yield the following expression for the number of cosmic ray bursts, N_3, which produce discharge-initiating electrons in the beam volume:

$$N_3 = \int_{H_2}^{H_3} D_B I \tau dR \qquad (5\text{-}10)$$

where H_2 and H_3 are the lower and upper altitude limits of Region 3. In addition, an expression for the number of cosmic ray bursts/cm^2-sec,

I, is used to replace the expression for natural radioactivity intensity. From available data on the rate of appearance of cosmic ray bursts vs. altitude, it is possible to develop an approximate analytic expression for this quantity. The variation of cosmic ray burst intensity with altitude is shown in Figure 71 of Reference 6. Using this data, the following approximate expressions for cosmic ray intensity is assumed:

$$I \begin{cases} = 2.4 \times 10^{-5} \text{ Io H}, & 2 \times 10^5 \leq H \leq 14 \times 10^5 \\ = 33.6 \text{ Io}, & 14 \times 10^5 \leq H \leq 50 \times 10^5 \end{cases} \qquad (5\text{-}11)$$

where H is in centimeters. It should be noted that these expressions give values of I everywhere greater than those given in Figure 71 of Reference 6. Therefore, estimates of N_3 based on these expressions will tend to be high. This is particularly true for the region above 14 km, where a constant level of I is assumed and cosmic ray data show a decreasing level with altitude.

To use equations (5-11), Io must be evaluated. An approximate value for Io can be developed by considering the average particle flux due to cosmic radiation at an altitude of 2 km and relating this to the average number of particles appearing per burst. The particle flux due to cosmic radiation at this altitude is approximately 0.02 particles/cm^2-sec. The average number of ionizing particles per burst is 10^6 particles per burst. Therefore, the rate of appearance of bursts at this altitude per cm^2-sec is:

2×10^{-8} bursts/cm^2-sec

Using equations (5-5) and (5-11) in equation (5-10), the number of cosmic ray bursts, N_3, which generate electrons which can initiate a discharge in the microwave pulse in Region 3 are:

$$N_3 = \frac{2.4 \times 10^{-5} I_o \tau_1}{\sin \theta} \int_{2 \times 10^5}^{14 \times 10^5} \left(D_D H + \frac{\alpha H^2}{\sin \theta} \right) dH + \frac{33.6 I_o \tau_2}{\sin \theta} \int_{14 \times 10^5}^{50 \times 10^5} \left[D_D + \frac{\alpha H}{\sin \theta} \right] dH \quad (5\text{-}12)$$

where D_D and H are in cms and τ_1 and τ_2 are approximate values for τ in the 2 to 14 km and 14 to 50 km regions, respectively. These values are determined in part by the lifetime of an electron burst and in part by the variation in the time of arrival of individual particles in a shower. They will vary from 10^{-7} to 10^{-4} seconds, according to altitude.

Integration of equation (5-12) yields

$$N_3 = \frac{2.4 \times 10^{-5} I_o \tau_1}{\sin \theta} \left[9.6 \times 10^{11} D_D + 0.92 \times 10^{18} \frac{\alpha}{\sin \theta} \right] + \frac{33.6 I_o \tau_2}{\sin \theta} \left[3.6 \times 10^6 D_D + 11.5 \times 10^{12} \frac{\alpha}{\sin \theta} \right] \quad (5\text{-}13)$$

Assuming the following values for a typical case

$I_o = 2 \times 10^{-8}$ bursts/cm^2-sec

$\tau_1 = 10^{-6}$ sec

$$\tau_2 = 10^{-5} \text{ sec}$$

$$\sin \theta = 0.5$$

$$D_D = 10^3 \text{ cm}$$

$$\alpha = 10^{-2}$$

yields

$$N_3 \cong 3$$

The corresponding probability, P_3, that an ionizing cosmic ray shower will produce one or more discharge-initiating electrons along the beam path is 0.95.

The preceding analyses are greatly simplified, but do indicate that atmospheric breakdown must be taken into account in superpower microwave transmission. The probability of electrons being available for breakdown initiation in Region 1 is not high. In Regions 2 and 3, however, this probability appears to be high, but must be emphasized that the analyses concern only breakdown initiation, and do not determine how breakdown occurring within the volume of the transmitted beam affects beam transmission. Breakdown may be confined to small volumes in space and scatter only small fractions of the beam power. There are other considerations which must be examined in detail, however, such as the possible propagation of breakdown along the direction of propagation of the beam.

SECTION VI

CONCLUSIONS

A. Summary of Program Results

The thirteen-month investigation of the statistics of nanosecond breakdown has led to the following significant results:

1. Development of a simple pulse generator capable of applying sub-nanosecond rise-time voltage pulses of over 25 kilovolts to a test gap. Gap fields of 300 kv/cm have been used in the test gap, and fields in excess of 500 kv/cm can be realized. The pulser is simple, rugged, and reliable. It can be used to gather statistical time lag data, to study electrode conditioning, and to study formative time.
2. Preliminary data on cathode emission at field strengths as high as 300 kv/cm (10 times E_s) have been obtained for five different metal surfaces. These data are required for future system designs in which pulse power levels will be in excess of breakdown thresholds.
3. Data on electrode "conditioning" to reduce cathode emission have been obtained. These data show that appropriate conditioning can lead to considerable reduction in cathode emission.
4. A preliminary analysis of atmospheric breakdown has been developed. This analysis indicates that this may not pose a serious problem on super-power transmission, although more detailed analysis is required.

B. Recommendations for Further Work

The current program has demonstrated the effectiveness of the experimental technique used to study breakdown statistics. The program can be extended to provide considerably more useful data and to develop more effective "conditioning" techniques. In addition, the analysis of free-space breakdown requires refinement. The following specific suggestions are made for further investigation:

1. Improve the voltage pulser to provide a higher repetition rate and greater ease of operation. The goal of this improvement would be to increase the data rate by a factor of 10 to 100.
2. Carry "conditioning" sparking to 10,000 to 100,000 shots. In the work accomplished under the present program, the "conditioning" was stopped at 1,000 shots. In some instances the emission was still decreasing significantly often at this point.
3. Place special emphasis on developing "conditioning" techniques with the more promising metals such as steel with a goal of reducing emission to 10^3 electrons/cm^2 at 300 kv/cm. This would demonstrate the feasibility of operating nanosecond microwave pulse generating devices at superpower levels with low probability of breakdown.
4. Investigate the effectiveness of dielectric films placed on cathodes in inhibiting discharge initiation.
5. Conduct a more detailed analysis of atmospheric breakdown statistics.
6. Analyse the propagation of a discharge initiated within the volume occupied by a superpower pulse in free space. In this study, experimental verification of the results of the analysis may be required.

REFERENCES

1. McDonald, D. F. and Brient, S. J., "Nanosecond Pulse Breakdown Initiation and Growth," ~~RADC-TDR-63-545~~ Dielectric Strength Note 20, (Jan. 1964)

2. Felsenthal, P. and Proud, J. M., "Nanosecond Pulse Breakdown in Gasses," ~~RADC-TDR-64-38~~ Dielectric Strength Note 21, (March 1964)

3. Gould, L. and Roberts, L. W., J. Appl. Phys. 27, 1162 (1956)

4. Rogowski, W., Arch F. Elekt. 16, 73 (1926)

5. Fletcher, R. C., Phys. Rev. 76, 1501 (1949)

6. Janossy, L., Cosmic Rays, Clarenden Press (1950)